Cdon mutation and fetal alcohol converge on Nodal signaling in a mouse model of holoprosencephaly

Mingi Hong[1], Annabel Christ[2], Anna Christa[2], Thomas E. Willnow[2], and Robert S. Krauss[1,*]

[1]Department of Cell, Developmental, and Regenerative Biology, Icahn School of Medicine at Mount Sinai, New York, NY 10029, USA; [2]Max-Delbruck-Center for Molecular Medicine, 13125 Berlin, Germany

*Corresponding Author:
Robert S. Krauss, Department of Cell, Developmental, and Regenerative Biology, Icahn School of Medicine at Mount Sinai, New York, NY 10029. Phone: 212-241-2177; Fax: 212-860-9279; e-mail: Robert.Krauss@mssm.edu

Abstract

Holoprosencephaly (HPE), a defect in midline patterning of the forebrain and midface, arises ~1 in 250 conceptions. It is associated with predisposing mutations in the Nodal and Hedgehog (HH) pathways, with penetrance and expressivity graded by genetic and environmental modifiers, via poorly understood mechanisms. CDON is a multifunctional co-receptor, including for the HH pathway. In mice, *Cdon* mutation synergizes with fetal alcohol exposure, producing HPE phenotypes closely resembling those seen in humans. We report here that, unexpectedly, Nodal, not HH, signaling is the point of synergistic interaction between *Cdon* mutation and fetal alcohol. Window-of-sensitivity, genetic, and in vitro findings are consistent with a model whereby brief exposure of *Cdon* mutant embryos to ethanol during gastrulation transiently and partially inhibits Nodal pathway activity, with consequent effects on downstream HH signaling during midline patterning. These results illuminate mechanisms of gene-environment interaction in a multifactorial model of a common birth defect.

52 **Introduction**

53 Many common structural birth defects appear to arise from a complex and ill-defined
54 combination of genetic and environmental factors (Krauss and Hong, 2016). The notion that
55 environmental agents affect penetrance and expressivity of predisposing mutations is
56 speculated to underlie many human congenital anomalies, but has been difficult to demonstrate.
57 Animal models are therefore required, but these have been slow to emerge. Some recent
58 successful examples are a zebrafish model of craniofacial defects (*Pdgfra* mutations and fetal
59 alcohol), and mouse models of scoliosis (Notch pathway mutations plus hypoxia), facial clefting
60 (*Pax3* mutations plus 2,3,7,8-tetrachlorodibenzodioxin (TCDD)), and holoprosencephaly
61 (Hedgehog pathway mutations and fetal alcohol) (Hong and Krauss, 2012; Kietzman et al.,
62 2014; McCarthy et al., 2013; Sparrow et al., 2012; Zalc et al., 2015).

63 Holoprosencephaly (HPE) is a common developmental defect in midline patterning of
64 the forebrain and/or midface (Muenke and Beachy, 2001). HPE occurs approximately once per
65 250 human conceptions, with an associated in utero lethality of ~97% (Leoncini et al., 2008;
66 Shiota and Yamada, 2010). HPE is characterized by an unbroken continuum of rostroventral
67 midline anomalies that range from complete failure to partition the forebrain into hemispheres
68 plus cyclopia, through progressively less severe defects including partially partitioned forebrain,
69 single nostril, and midface hypoplasia (Cohen, 2006; Krauss, 2007; Muenke and Beachy, 2001).

70 Development of the rostroventral midline is initiated by signals derived from the
71 prechordal plate (PCP) (Kiecker and Niehrs, 2001; Marcucio et al., 2011). The PCP produces
72 Sonic hedgehog (SHH), initiating a sequence of events that progressively patterns the forebrain
73 and midface. *Shh* is expressed in a temporal cascade: first in the PCP, subsequently in the
74 ventral midline of the diencephalon and telencephalon, and finally in the midfacial ectoderm
75 (Aoto et al., 2009; Cordero et al., 2004; Geng and Oliver, 2009; Kiecker and Niehrs, 2001;
76 Rubenstein and Beachy, 1998; Zhang et al., 2006). SHH induces midline cell fates and
77 structures throughout this process. HH ligands initiate signaling by binding the primary receptor

78 Patched1 (PTCH1). In the absence of ligand, PTCH1 constrains the activity of a second
79 membrane protein, Smoothened (SMO). HH binding inhibits PTCH1 function, allowing SMO-
80 dependent signals to activate GLI transcription factors and pathway-specific gene expression.
81 HH ligand availability and signal reception are also regulated by a series of co-receptors and
82 additional HH-binding proteins, including CDON, BOC, GAS1, and LRP2 (Beachy et al., 2010;
83 Kong et al., 2019; Lee et al., 2016; Petrov et al., 2017; Willnow and Christ, 2017).

84 The PCP develops from the anterior primitive streak (APS) under the influence of Nodal
85 pathway signaling (Robertson, 2014; Schier, 2009; Shen, 2007). Therefore, the Nodal pathway
86 is developmentally upstream of the HH pathway in rostroventral midline patterning. Consistent
87 with this conclusion, defective Nodal signaling at the primitive streak stage of development
88 leads to defects in HH signaling and HPE (Krauss, 2007). Nodal is a TGFβ superfamily member
89 and signals through a receptor complex including the type I and type II receptors, ALK4 and
90 Activin receptor IIA/B (ActRIIA/B), and a GPI-linked co-receptor, Cripto (Robertson, 2014;
91 Schier, 2009; Shen, 2007). Receptor activation results in phosphorylation of the transcription
92 factors SMAD2 and SMAD3, and activation of genes required for PCP induction (Robertson,
93 2014; Schier, 2009; Shen, 2007). Among these genes are *FoxA2* and *Gsc* (Ang and Rossant,
94 1994; Belo et al., 1998; Filosa et al., 1997). Nodal signaling also induces expression of *Lefty1*
95 and *Lefty2*, which encode secreted inhibitors of the pathway that bind to Cripto and Nodal itself
96 (Robertson, 2014; Schier, 2009; Shen, 2007).

97 The etiology of HPE is complex, involving both genetic and environmental risk factors
98 (Dubourg et al., 2018; Hong and Krauss, 2018; Johnson and Rasmussen, 2010; Krauss, 2007;
99 Miller et al., 2010; Muenke and Beachy, 2001; Roessler et al., 2018a; Roessler et al., 2018b;
100 Summers et al., 2018). Heterozygous, loss-of-function mutations in components or regulators of
101 the HH, Nodal, and FGF signaling pathways are associated with HPE (Roessler et al., 2018a;
102 Roessler et al., 2018b). Epidemiology of HPE is less advanced than genetic analyses, but

among the environmental risk factors implicated is fetal alcohol exposure (Abe et al., 2018; Cohen and Shiota, 2002; Croen et al., 2000). A full range of clinical phenotypes is observed in both sporadic and familial HPE (Muenke and Beachy, 2001; Solomon et al., 2010). Many mutation carriers in pedigrees lack clinical manifestation, and many apparently sporadic cases have inherited a mutation from a minimally affected parent (Lacbawan et al., 2009; Solomon et al., 2012). It is likely, therefore, that HPE-associated mutations are not sufficient to produce midline defects, but are the substrate on which a complex landscape of genetic and/or environmental modifiers act. Statistical analysis is consistent with a multifactorial, "autosomal dominant with modifier" model, wherein the penetrance and expressivity of a heterozygous driver mutation is graded by the modifier landscape (Dubourg et al., 2018; Hong and Krauss, 2018; Roessler et al., 2012).

We have modeled this phenomenon in mice with high fidelity. *CDON* encodes a multi-functional co-receptor, including for the HH pathway, (Lu and Krauss, 2010; Sanchez-Arrones et al., 2012), and *CDON* mutations are associated with human HPE (Bae et al., 2011; Roessler et al., 2018a). *Cdon*$^{-/-}$ mice on a 129S6 genetic background have a subthreshold defect in HH signaling and are subject to HPE induced by genetic and environmental modifiers; among the latter is ethanol (EtOH) (Hong and Krauss, 2018). *Cdon* mutation or in utero EtOH exposure individually yielded little effect on 129S6 mice; the combination, however, synergized to inhibit HH signaling in the developing forebrain and produced a complete spectrum of HPE phenotypes with high penetrance (Hong and Krauss, 2012). Furthermore, fetal EtOH induced a low penetrance of HPE in C57BL/6J mice, and this was exacerbated by heterozygosity for *Shh* or *Gli2* (Kietzman et al., 2014). Consistent with the notion that a threshold of HH signaling activity is rate-limiting in midline patterning, genetic removal of one copy of the negative pathway regulator, *Ptch1*, rescued 129S6 *Cdon*$^{-/-}$ mice from EtOH-induced HPE (Hong and Krauss, 2013).

128 Defective HH pathway function may be a final common mechanism for all classical forms
129 of HPE, so these results do not prove that HH signaling is the direct synergistic target of *Cdon*
130 mutation and in utero EtOH exposure. Several lines of evidence argue that EtOH itself, rather
131 than a consequence of its metabolism, is the HPE-inducing teratogen (Hong and Krauss, 2017).
132 In this study, we demonstrate that the window of sensitivity to EtOH-induced HPE in 129S6
133 *Cdon*$^{-/-}$ mice is closed by embryonic day (E) 7.5, prior to *Shh* expression in the PCP (Echelard et
134 al., 1993). The sensitivity period of EtOH-induced HPE overlaps with Nodal-mediated
135 specification of the PCP from the APS. Furthermore, we find that CDON interacts genetically
136 and physically with regulators of Nodal signaling. Finally, EtOH inhibits Activin/Nodal pathway
137 signaling in vitro in mouse epiblast stem cells (mEpiSCs), which have transcriptional and
138 functional properties that resemble APS cells (Kojima et al., 2014; Tsakiridis et al., 2014).
139 Together these results argue that, unexpectedly, *Cdon* mutation and fetal alcohol synergize to
140 induce HPE by interfering with Nodal signaling. These results illuminate mechanisms of gene-
141 environment interaction in a high fidelity, multifactorial model of a common birth defect.
142

143 **Results**

144 **The window of sensitivity to EtOH-induced HPE coincides with Nodal, not Hh, signaling**

145 All studies were performed with mice on a 129S6 background and are referred to only by
146 genotype unless otherwise noted. Our model uses one-hour timed mating of *Cdon*$^{+/-}$ mice,
147 allowing rigorous identification of a window of sensitivity for EtOH's teratogenic effects. The
148 standard EtOH treatment regimen involves one dose at E7.0 and a second dose four hours
149 later; this results in a full range of HPE phenotypes in *Cdon*$^{-/-}$ mice with overall penetrance of
150 ~75% (Hong and Krauss, 2012). The protocol is analogous to the original regimen developed to
151 model fetal alcohol spectrum disorders in C57BL/6J mice, wherein ~19% developed HPE
152 phenotypes (Aoto et al., 2008; Sulik et al., 1981). HPE phenotypes were not induced in wild type
153 C57BL/6J mice when EtOH was administered at E6.5 or E7.5 (Aoto et al., 2008). We have
154 shown that EtOH is ineffective in *Cdon*$^{-/-}$ mice when administered at E8.0 (Hong and Krauss,
155 2012). To further refine the temporal window of sensitivity, we assessed the ability of EtOH to
156 induce HPE in *Cdon*$^{-/-}$ animals when administered at E7.25 and E7.5, with embryos examined
157 for external HPE phenotypes at E14.0. EtOH was effective at E7.25, but not at E7.5 (Table 1).

158 EtOH itself is the HPE-inducing teratogen in this system (Hong and Krauss, 2017). The
159 developmental processes directly perturbed by EtOH must therefore occur: 1) during the
160 sensitive time window; and 2) prior to EtOH clearance, even if defects in midline development
161 occur later. *Shh* expression in the midline begins at E7.5-E7.75 (Echelard et al., 1993). When
162 administered at E7.0, maternal blood EtOH levels peaked at E7.25 and were no longer
163 detectable by ~E7.75 (Hong and Krauss, 2012). Critically, EtOH is no longer effective at E7.5, a
164 time prior to SHH function in prechordal plate-mediated rostroventral midline patterning
165 (Echelard et al., 1993; McMahon et al., 2003). Therefore, it is very unlikely that direct inhibition
166 of HH signaling is the mechanism of EtOH-induced HPE. Consistent with this conclusion, the
167 time of peak sensitivity to HPE induced by the direct SMO inhibitor, Vismodegib, was E7.5, 6 –
168 12 hours later than for EtOH (Heyne et al., 2015).

169 Both the window of sensitivity to EtOH and peak EtOH levels overlap with induction of
170 the PCP by Nodal signaling. We previously observed that expression of *FoxA2* and *Gsc*, genes
171 regulated by Nodal that mark the APS (from which the PCP is derived), was diminished at E7.25
172 in EtOH-treated *Cdon*$^{-/-}$ embryos. Both *Cdon* mutation and EtOH exposure were required for this
173 effect (Hong and Krauss, 2012). Expression of *Lefty2*, a direct Nodal pathway target gene, was
174 also reduced at E7.25 specifically in EtOH-treated *Cdon*$^{-/-}$ embryos (Figure 1). Taken together,
175 these results showed that the synergy between *Cdon* mutation and in utero EtOH exposure
176 occurred during Nodal-dependent specification of the PCP and that reduction of Nodal target
177 gene expression required a combination of mutation and teratogen. The observation that loss of
178 CDON was required for the effect suggests that, in addition to its role as a SHH co-receptor,
179 CDON functions earlier in development to promote midline patterning, potentially via the Nodal
180 pathway. In fact, *Cdon* expression initiates during gastrulation and is seen in embryonic
181 mesoderm and ectoderm (Hong and Krauss, 2012; Mulieri et al., 2000).
182
183 ***Cdon* interacts genetically with Nodal pathway components**
184 Mice with mutations resulting in complete loss of Nodal signaling gastrulate abnormally and die
185 early in development, but hypomorphic pathway mutants display a range of HPE phenotypes
186 (Andersson et al., 2006; Chu et al., 2005; Lowe et al., 2001; Nomura and Li, 1998; Schier, 2009;
187 Shen, 2007; Song et al., 1999). To further probe the linkage between CDON and regulation of
188 Nodal signaling, we assessed whether *Cdon* interacted genetically with *Cripto* and *Lefty2*, direct
189 positive and negative regulators of the Nodal pathway, respectively. When analyzed at E10,
190 ~14% of *Cdon*$^{-/-}$ embryos treated with EtOH had alobar HPE and cyclopia, dying in utero by E11
191 (Hong and Krauss, 2012, 2013). When studied at E14, ~70% of such embryos displayed lobar
192 HPE and a range of craniofacial midline phenotypes, including fused upper lip and single nostril
193 (Hong and Krauss, 2012, 2013). To address genetic interactions between *Cdon* and Nodal

194 pathway regulators, we took advantage of the high penetrance of phenotypes at E14 and
195 analyzed embryos at this stage for these unambiguous, easily scored phenotypes.
196 Targeted mutations in *Cripto* and *Lefty2* (Ding et al., 1998; Meno et al., 1999) were
197 placed onto the 129S6 genetic background and then crossed to *Cdon* mutants to generate
198 double heterozygotes. Offspring of intercrosses of these mice were further crossed and
199 pregnant females were treated with EtOH or saline as a control. *Cripto* is essential for Nodal
200 signaling. *Lefty2* is induced in response to Nodal signaling to provide critical negative feedback
201 as an inhibitor of the pathway. Since CDON and EtOH may act together at the level of Nodal
202 signaling in HPE, we predicted that removal of one copy of *Cripto* would sensitize *Cdon*$^{-/-}$
203 embryos to EtOH-induced HPE. In contrast, removal of one copy of *Lefty2* would be predicted to
204 rescue *Cdon*$^{-/-}$ embryos from EtOH-induced HPE. (Null mutations in *Cripto* and *Lefty2* result in
205 early lethality due to strong gastrulation defects (Ding et al., 1998; Meno et al., 1999), so
206 studying homozygous double mutants with *Cdon* is impossible.) To permit the detection of
207 sensitization by *Cripto* heterozygosity, we used a dose of EtOH which we previously reported
208 gives ~30% penetrance of HPE at E14 (2.9 g/kg) (Hong and Krauss, 2012). With this regimen,
209 28% of EtOH-treated *Cdon*$^{-/-}$;*Cripto*$^{+/+}$ embryos had HPE, whereas 55% of *Cdon*$^{-/-}$;*Cripto*$^{+/-}$
210 embryos did ($p<0.014$) (Table 2, Figure S1). With the exception of a single EtOH-treated
211 *Cdon*$^{+/-}$;*Cripto*$^{+/-}$ embryo, EtOH-treated mice of other genotypes and saline-treated control mice
212 did not display HPE. Removal of one copy of *Cripto* therefore sensitized *Cdon*$^{-/-}$ mice to EtOH-
213 induced HPE.
214 *Nodal*$^{-/-}$ and *Lefty2*$^{-/-}$ embryos have opposite defects in gastrulation and display dosage-
215 dependent genetic interactions, with *Lefty2* functioning as a negative regulator of the pathway
216 (Meno et al., 1999). To test for phenotypic suppression in EtOH-induced HPE, we used the
217 standard dose of EtOH (3.48 g/kg) for these analyses, as it results in high penetrance. All
218 embryos with HPE at E14 display a fused upper lip, while only some show the more severe
219 single nostril phenotype. Approximately 70% of EtOH-treated *Cdon*$^{-/-}$;*Lefty2*$^{+/+}$ embryos had a

220 fused upper lip, similar to our previous findings (Hong and Krauss, 2012, 2013), whereas 54%
221 of *Cdon*$^{-/-}$;*Lefty2*$^{+/-}$ embryos did, revealing a trend toward overall reduction of HPE frequency
222 (p=0.14). However, while 21% of EtOH-treated *Cdon*$^{-/-}$;*Lefty2*$^{+/+}$ embryos had a single nostril,
223 only 6% of *Cdon*$^{-/-}$;*Lefty2*$^{+/-}$ embryos did ($p<0.05$) (Table 3, Figure S1). Again, EtOH-treated
224 mice of other genotypes and saline-treated control mice did not display HPE. Therefore,
225 removal of one copy of *Lefty2* rescued a more severe form of HPE associated with EtOH
226 treatment. Taken together, these studies revealed that the Nodal signaling components *Cripto*
227 and *Lefty2* act as heterozygous enhancer and suppressor genes, respectively, of EtOH-induced
228 HPE in *Cdon*$^{-/-}$ embryos.
229

230 **EtOH inhibits Activin/Nodal signaling in mEpiSCs**

231 The APS is a small, transiently existing cell population, making it hard to study directly. Cultured
232 mEpiSCs have transcriptional and functional properties resembling APS cells (Kojima et al.,
233 2014; Tsakiridis et al., 2014), making them a tractable in vitro surrogate model. mEpiSCs rely on
234 FGF2 and Activin/Nodal signaling for maintenance as self-renewing, pluripotent stem cells
235 (Brons et al., 2007; Vallier et al., 2009). Activin A and Nodal use the same receptor and
236 signaling mechanism, except that Nodal, but not Activin A, requires the co-receptor Cripto.
237 Therefore, we evaluated the effects of EtOH on Activin/Nodal signaling in mEpiSCs.

238 A direct readout of Nodal signaling activity is receptor-mediated phosphorylation of
239 SMAD2 at its C-terminus (Robertson, 2014; Schier, 2009; Shen, 2007). We assessed C-
240 terminally phosphorylated SMAD2 (p-SMAD2C) and total SMAD2 levels in the mEpiSC line,
241 EpiSC9 (Najm et al., 2011), after treatment with EtOH for 6 hours. A relatively short treatment
242 duration was chosen because: 1) the in vivo model is an acute exposure regimen; 2) the
243 window of sensitivity to EtOH-induced HPE is <12 hours; and 3) high EtOH levels last only

244 about 10 hours in pregnant females (Hong and Krauss, 2012). EtOH dose-dependently
245 diminished p-SMAD2C levels in mEpiSCs, without altering total SMAD2 levels (Figure 2A, B).
246 EtOH stimulates activation of the MAP kinase, JNK, in specific cell types (McAlhany et
247 al., 2000; Ren et al., 2017). SMAD2 is phosphorylated in its linker region by MAP kinases
248 (Massagué, 2003; Rezaei et al., 2012), usually leading to inhibition of SMAD2 function (Grimm
249 and Gurdon, 2002; Kretzschmar et al., 1999; Lessard et al., 2018). We therefore assessed total
250 and phosphorylated (activated) forms of JNK1 MAP kinase in EtOH-treated mEpiSCs. EtOH
251 dose-dependently increased phospho-JNK1 (T183/Y185) levels (p-JNK1; Figure 2A, B).
252 Consistent with EtOH-induced p-JNK1 activation, phosphorylation of the SMAD2 linker region
253 (p-SMAD2L) also occurred in an EtOH dose-dependent manner, with production of p-JNK1 and
254 p-SMAD2L correlating well (Figure 2A, B).
255 Human embryonic stem cells (hESCs) resemble mEpiSCs (Pauklin and Vallier, 2015).
256 Treatment of hESC or mEpiSC cultures with the ALK4 inhibitor, SB43152, led to reduction of
257 Activin/Nodal target gene expression and, eventually, induction of early markers of
258 neuroectoderm differentiation (Chng et al., 2010; Li et al., 2015; Liu et al., 2018; Vallier et al.,
259 2009). These studies generally used time courses of days to weeks, but Vallier et al. assessed
260 expression of five Activin/Nodal target and/or pluripotency-related genes in hESCs treated with
261 SB43152 for 6 hours, the same amount of time we treated mEpiSCs with EtOH. Levels of
262 *Nanog*, *Nodal*, and *LeftyA* mRNA were reduced by SB43152, whereas levels of *Oct4* and *Sox2*
263 underwent little or no change (Vallier et al., 2009). We assessed expression of these five genes
264 in mEpiSCs treated with EtOH for 6 hours (Figure 2C). Similar to SB43152-treated hESCs,
265 EtOH-treated mEpiSCs displayed significantly reduced levels of *Nanog* and *Nodal* mRNAs,
266 while *Oct4* and *Sox2* mRNA levels were largely unchanged. Expression of the additional
267 SB43152-inhibitable mEpiSC markers *Fgf5* and *T* (Liu et al., 2018) were also reduced by EtOH
268 treatment (Figure 2C). In contrast, EtOH did not alter levels of *Lefty1* or *Lefty2* in mEpiSC
269 cultures (Figure S2). As these are known Activin/Nodal target genes, this result might be related

270 to differences in SB43152 vs. EtOH treatment, or differences in half-lives of these mRNAs in
271 human vs. mouse cultures. Therefore, acute EtOH treatment of mEpiSCs resulted in an
272 inhibitory SMAD2 phosphorylation pattern and changes in gene expression similar to those
273 induced by a direct Activin/Nodal pathway inhibitor. Induction of neuroectoderm-specific genes
274 (e.g., *HoxA1*, *Six1*, and *Gbx2*) was observed in hESCs treated with SB43152 for 2 – 6 days
275 (Chng et al., 2010; Vallier et al., 2009). After 6 hours of EtOH treatment, we found a varied
276 response, with *HoxA1* levels strongly induced, *Six1* expression displayed a biphasic dose-
277 response, and *Gbx2* levels reduced (Figure S2).
278

279 ***Cdon* and *Lrp2* genetically interact in mice to generate phenotypes resembling Nodal**
280 **pathway hypomorphs, and both bind to Cripto**

281 Our findings argue that CDON plays an earlier role in development than its known function as a
282 SHH co-receptor. The need for EtOH exposure to reveal this role suggests that CDON's effects
283 in primitive streak embryos may be redundant with other factors. The Hh co-receptors BOC and
284 GAS1 are not likely to be such factors, as *Cdon;Boc;Gas1* triple knockout mice had a phenotype
285 that is close to a complete loss of embryonic HH pathway function, but not Nodal pathway-like
286 phenotypes (Allen et al., 2011). LRP2 is an endocytic and auxiliary receptor for multiple
287 morphogenetic ligands and receptors (Willnow and Christ, 2017). *Lrp2*$^{-/-}$ mice have HPE of
288 variable penetrance and severity (Christ et al., 2012; Spoelgen et al., 2005; Willnow and Christ,
289 2017; Willnow et al., 2012)**.** We therefore constructed mice with mutations in *Cdon* and *Lrp2*.
290 Some *Cdon;Lrp2* double mutants at E11.5 had a severe truncation of anterior head and face
291 structures, a phenotype neither single mutant displayed (Figure 3A). Surviving embryos
292 displayed a range of phenotypes, including milder craniofacial truncation and strong HPE
293 (Figure 3B, C). Loss of anterior head structure is a more severe phenotype than that seen even
294 in *Smo* mutants, which lack all HH signaling (Zhang et al., 2001). These phenotypes – anterior

295 truncations and HPE – are similar to those observed in mice with partial loss of Nodal pathway
296 function (e.g., hypomorphic *Nodal* and *Cripto* mutants, and *Nodal*$^{+/-}$;*Smad2*$^{+/-}$ mutants, each
297 have phenotypes that include truncation of anterior head structures and severe HPE)
298 (Andersson et al., 2006; Chu et al., 2005; Lowe et al., 2001; Nomura and Li, 1998; Song et al.,
299 1999). The *Cdon*/*Lrp2* genetic interaction is specific and selective: the *Cdon* paralog *Boc* is not
300 expressed in primitive streak-stage embryos (Mulieri et al., 2002; Zhang et al., 2001), and *Boc*
301 mutant mice do not synergize with *Lrp2* mutants (unpublished results), nor are they sensitive to
302 EtOH-induced HPE (Hong and Krauss, 2012).
303 CDON is a multifunctional co-receptor and promotes SHH-independent signaling when
304 associated with various other receptors and cell adhesion molecules. In addition to binding HH
305 ligands and PTCH1, CDON interacts with and influences signaling by classical cadherins; the
306 Netrin receptor, Neogenin; and the WNT co-receptor, LRP6 (Bae et al., 2011; Bae et al., 2009;
307 Izzi et al., 2011; Jeong et al., 2014; Kang et al., 2003; Kang et al., 2004; Lu and Krauss, 2010;
308 Tenzen et al., 2006). We hypothesized that CDON might work similarly in Nodal signaling. To
309 address this possibility, we assessed whether CDON binds to Nodal receptor components. A
310 secreted CDON ectodomain fused in-frame at its carboxy terminus with the IgG Fc region
311 (CDON-Fc) was expressed in HEK293T cells with individual ectodomains of the Nodal receptor
312 (ActRIIA, ActRIIB, ALK4, and Cripto) fused in-frame at their carboxy termini with alkaline
313 phosphatase (AP). As positive and negative controls, SHH-N-AP and CD164-AP were used,
314 respectively (SHH-N is the active portion of SHH, CD164 is a cell surface sialomucin) (Kang et
315 al., 2002; Tenzen et al., 2006). The use of secreted ectodomains reduces the possibility that
316 unknown, cell surface bound factors promote binding or contribute directly to the complex.
317 Conditioned medium was collected, and equivalent amounts of AP fusion proteins from
318 conditioned media were pulled down and blotted for captured CDON-Fc. Conversely, equivalent
319 levels of Fc were pulled down, and associated AP activity was quantified. Similar results were
320 obtained in each pull-down: CDON-Fc interacted efficiently with Cripto-AP, similar to the

321 interaction between CDON-Fc and SHH-N-AP (Figure 4A, B). CDON-Fc did not bind to the
322 negative control CD164-AP, and it interacted only weakly with the AP-tagged versions of ALK4,
323 ActRIIA, and ActRIIB (Figure 4A, B).

324 As CDON and LRP2 interacted genetically to produce Nodal hypomorph-like
325 phenotypes, we asked whether LRP2, like CDON, binds to Cripto. The extracellular region of
326 LRP2 harbors four repetitive modules, each comprising a cluster of complement-type repeats
327 followed by EGF-type repeats and β-propellers. Each module is likely capable of independently
328 binding ligands, as shown for the related receptor, LRP1 (Croy et al., 2003). LRP2 is a huge
329 polypeptide of 4660 amino acids, making it difficult to express in vitro. Therefore, we
330 constructed a series of soluble "mini-receptors" (designated sR1, sR2, sR3, and sR4) spanning
331 virtually the entire ectodomain in four non-overlapping pieces, each fused in-frame at their
332 carboxy termini to the IgG Fc region (see Figure 4C). Each soluble ectodomain segment and
333 Cripto-Fc were expressed in HEK293T cells and assessed for their ability to bind to each other.
334 LRP2 binds SHH-N (Christ et al., 2012; McCarthy et al., 2002), so this ligand was used again as
335 a positive control, with CD164-AP serving as a presumptive negative control. Each soluble
336 LRP2 mini-receptor ectodomain (i.e., sR1 to sR4) pulled down SHH-N-AP, revealing that LRP2
337 harbors multiple SHH-N binding sites (Figure 4D). These results were confirmed by expressing
338 each ectodomain segment joined with the native LRP2 transmembrane and cytoplasmic
339 domains (mini-receptors R1, R2, R3, and R4; Figure 4C) in NIH3T3 cells. These cultures were
340 incubated with recombinant SHH-N-GST fusion proteins for 2 hours, followed by
341 immunoprecipitation with anti-LRP2 antibody recognizing all mini-receptors and Western blotting
342 with antibodies to LRP2 or GST. Again, all four mini-receptors pulled down SHH-N, whereas no
343 pulldown of SHH-N was seen in control transfectants lacking LRP2 mini-receptors (Figure 4E).
344 Finally, we assessed LRP2 binding to Cripto with the soluble ectodomain binding assay. Similar
345 to its multivalent interaction with SHH-N, each soluble LRP2 ectodomain segment (sR1 to sR4)

346 pulled down Cripto-AP (Figure 4D). The efficiency of LRP2 mini-receptor ectodomains to bind

347 SHH-N-AP and Cripto-AP was similar to that of CDON-Fc (Figure 4D).

348

349 **Discussion**

350 HPE is a common developmental disorder, but its etiology remains poorly understood.
351 Mutations in the Nodal, HH, and FGF pathways are associated with HPE (Roessler et al.,
352 2018a), but these alone are insufficient to drive aberrant development. Identifying and
353 understanding the critical phenotypic modifiers of such mutations is important but still in its
354 infancy. Many birth defects are thought to be caused by poorly defined interactions between
355 genetic and environmental risk factors, but the mechanistic bases of these interactions are
356 largely unknown (Krauss and Hong, 2016). *Cdon* mutation and fetal alcohol are each implicated
357 in human HPE (Abe et al., 2018; Bae et al., 2011; Cohen and Shiota, 2002; Croen et al., 2000;
358 Roessler et al., 2018a). The *Cdon* mutation plus fetal alcohol model is noteworthy for its
359 specificity and fidelity to many aspects of human HPE (Hong and Krauss, 2012). Therefore,
360 illumination of how loss of *Cdon* interacts with in utero EtOH exposure provides insight into
361 mechanisms of HPE and how fetal alcohol functions as a teratogen in this anomaly.

362 The Nodal pathway is developmentally upstream from the HH pathway in patterning the
363 rostroventral midline. While CDON is clearly a component of the HH pathway, it regulates
364 signaling within several additional pathways as well (Bae et al., 2011; Bae et al., 2009; Izzi et
365 al., 2011; Jeong et al., 2014; Kang et al., 2003; Kang et al., 2004; Lu and Krauss, 2010; Tenzen
366 et al., 2006). Multiple lines of evidence presented here argue that CDON also regulates Nodal
367 signaling and that the Nodal pathway is the point of synergistic interaction between mutation of
368 *Cdon* and fetal EtOH exposure. The evidence includes: 1) EtOH-treated *Cdon*$^{-/-}$ embryos display
369 defects in expression of Nodal target genes in the APS, whereas EtOH treatment or *Cdon*
370 mutation alone do not; 2) the window of sensitivity to EtOH-induced HPE is very narrow and
371 closed by E7.5, prior to *Shh* function in rostroventral midline patterning; 3) EtOH itself is the
372 likely HPE-inducing teratogen and peak circulating EtOH levels coincide with Nodal signaling in
373 the APS; 4) *Cdon* interacts genetically with the critical Nodal pathway factors *Cripto* and *Lefty2*
374 in EtOH-induced HPE; 5) acute EtOH treatment dose-dependently diminishes p-SMAD2C and

375 elevates p-SMAD2L levels, and inhibits Activin/Nodal-dependent gene expression in mEpiSCs;
376 6) *Cdon;Lrp2* double mutants display phenotypes similar to mice with hypomorphic Nodal
377 pathway mutations, including anterior truncations, a phenotype not seen in mice lacking all HH
378 signaling; and 7) CDON and LRP2 both bind efficiently to Cripto, an essential component of the
379 Nodal receptor.

380 Together our findings are consistent with the following model: CDON and LRP2 function
381 with overlapping or compensatory roles to regulate Nodal pathway signaling in the APS during
382 induction of the PCP. Brief exposure of *Cdon*$^{-/-}$ embryos to EtOH during this period transiently
383 and partially inhibits Nodal pathway activity. While all the mice successfully gastrulate, they
384 emerge from this period predisposed towards development of HPE in a stochastic manner. If
385 HH signaling strength fails to reach a required threshold early during rostroventral midline
386 patterning, at the PCP stage, the outcome is alobar HPE and cyclopia; if it occurs at later stages
387 of development, the outcomes are progressively less severe. Aspects of the model will require
388 additional experimentation, but it is logically consistent with the synergistic effects of fetal
389 alcohol and *Cdon* mutation within a narrow window of sensitivity, and also with the "mutation
390 plus modifier" view of human HPE.

391 The specific mechanisms whereby acute EtOH treatment reduces expression of Nodal
392 target genes in the APS of *Cdon*$^{-/-}$ mice and diminishes Activin/Nodal signaling in mEpiSCs are
393 not known. EtOH itself, rather than consequences of its oxidative metabolism, is very likely the
394 HPE-inducing teratogen (Hong and Krauss, 2017). An alternative mechanism to metabolism-
395 based toxicity is that EtOH itself functions to perturb cell membranes via its hydrophobicity
396 (Lyon et al., 1981; McCarns et al., 1997). One possibility is that EtOH's hydrophobic nature
397 perturbs trafficking of Nodal receptor components or their stable assembly at the cell surface.
398 Cripto is a GPI-linked protein, so might be especially vulnerable to hydrophobic membrane
399 perturbation. However, exogenously provided Activin A is the major activator of SMAD2 in

400 cultured mEpiSCs, and Activin does not require Cripto to signal through ActRII/Alk4. EtOH
401 reduces p-SMAD2C levels in these cultures, so Cripto may not be a direct critical target of
402 EtOH. Nevertheless, mEpiSCs endogenously express Nodal (Kojima et al., 2014), which does
403 require Cripto, and its contribution to SMAD2 signaling in these cultures is not fully clear.
404 Additionally, EtOH activates JNK1 in mEpiSCs, with a corresponding increase in p-SMAD2L
405 levels. Phosphorylation of SMAD2 by MAP kinases is generally inhibitory to SMAD2 activity,
406 independent of p-SMAD2C phosphorylation status (Massagué, 2003; Rezaei et al., 2012), so
407 EtOH appears to promote or inhibit multiple signals that converge on SMAD2 phosphorylation.

408 CDON regulates several signaling pathways, but it has not previously been implicated in
409 Nodal signaling. How CDON functions to regulate Nodal signaling is of obvious interest.
410 *Cdon;Lrp2* double mutant mice display phenotypes that resemble Nodal pathway hypomorphs,
411 and CDON and LRP2 each bind to Cripto. Therefore, as with the effects of EtOH, Cripto is a
412 possible point of regulation. One potential mechanism is that CDON and LRP2 might function as
413 components of a larger Nodal receptor complex, contributing via interaction with Cripto.
414 Alternatively, they may work with Cripto in processing and trafficking of Nodal or other receptor
415 components, or play a role in processing and trafficking of Cripto itself (Constam, 2009). There
416 is evidence in other systems that CDON and LRP2 can act in such a manner. LRP2 is best
417 understood as an endocytic receptor that controls internalization and intracellular trafficking of
418 both soluble and membrane-bound proteins, including PTCH1, the Na^+/H^+ exchanger NHE3,
419 and the intrinsic factor receptor, cubilin (Willnow and Christ, 2017). Furthermore, CDON
420 regulates subcellular localization of N-cadherin during neural crest migration in zebrafish
421 (Powell et al., 2015). Similarly, the *Drosophila* orthologs of CDON act not only as co-receptors
422 for HH, but in trafficking of the primary HH receptor, PTC (Zheng et al., 2010). Another
423 possibility is in regulation of cell-cell contact and adhesion. CDON is localized to sites of cell-cell
424 contact and functions with N-cadherin in cell adhesion-dependent signaling (Kang et al., 2003;

425 Lu and Krauss, 2010). In zebrafish, a positive feedback loop exists between Nodal signaling, E-
426 cadherin expression, and duration of cell-cell contact that directs PCP specification, at the
427 expense of endoderm specification (Barone et al., 2017). It is conceivable that CDON could play
428 a role in adhesion-mediated, higher order regulatory events like this as well. These varied
429 potential mechanisms are not mutually exclusive.

430 Our findings offer insight into how *Cdon* mutation synergizes with fetal alcohol in mice to
431 produce a wide spectrum of HPE phenotypes, closely resembling the complex etiology and
432 variable outcomes seen in humans at the population level. A combination of approaches,
433 including window of sensitivity studies, genetic interactions in mice, and in vitro analyses
434 revealed that, unexpectedly, the point of synergy is at the level of Nodal, not HH, signaling.
435 These findings illuminate gene-environment interactions in the causation of a common birth
436 defect and serve as a conceptual framework for additional developmental anomalies.
437
438

439 **Materials and Methods**

440 **Mice**

441 All animal procedures were conducted in accordance with institutional guidelines for the care
442 and use of laboratory animals as approved by the Institutional Animal Care and Use Committee
443 (IACUC) of the Icahn School of Medicine at Mount Sinai and according to Max-Delbruck-Center
444 guidelines following approval by local authorities (X9007/17). B6.129P2-*Lefty2*^{tm1Hmd} mice were
445 provided by Hiroshi Hamada. *Cripto-LacZ* mice were provided by Michael Shen. Both strains
446 were transferred onto the 129S6/SvEvTac (129S6) background with the Taconic Speed
447 Congenic Program, by backcrossing and mapping with the 1450 SNP array. Mice used for these
448 experiments were estimated to be over 98% 129S6/SvEvTac background. These lines were
449 crossed with *Cdon*$^{+/tm1Rsk}$ (*Cdon*$^{+/-}$) mice on the 129S6 background (Cole and Krauss, 2003;
450 Hong and Krauss, 2012) to generate 129S6.*Cdon*$^{+/-}$;*Lefty2*$^{+/-}$ and 129S6.*Cdon*$^{+/-}$*Cripto*$^{+/-}$ double-
451 mutant mice. Because *Cdon* and *Cripto* are both located on chromosome 9, *Cdon*$^{+/-}$;*Cripto*$^{+/-}$
452 mice were crossed with wild type mice and offspring screened for those that carried a
453 recombinant chromosome 9 carrying both *Cdon* and *Cripto* mutant alleles. Offspring of
454 intercrosses of these mice were further crossed (see Tables 2 and 3 for details) and pregnant
455 females treated with EtOH or saline as a control (Hong and Krauss, 2012). Briefly, two- to three-
456 month old mice were mated for one hour in the dark and plugged females were collected. The
457 time of the plug was designated as embryonic day (E) 0.0. Pregnant female mice were injected
458 intraperitoneally twice with 15 μl per g body weight of solution of 30% EtOH in saline (3.48 g/kg)
459 at E7.0 and again 4 hours later, with the exception of studies involving *Cdon;Cripto* mutants. For
460 these experiments, a lower dose of ethanol (25% EtOH in saline, 2.9 g/kg) was used. Saline
461 injections were used as controls.

462 Mice with targeted gene disruption of *Lrp2* (*Lrp2*^{tm1Her}) have been described (Willnow et
463 al., 1996). *Lrp2*$^{+/tm1Her}$ (*Lrp2*$^{+/-}$) mice were kept on the C57BL/6N genetic background and

464 crossed with *Cdon*$^{+/-}$ mice on the C57BL/6N genetic background. Offspring were further
465 intercrossed, and *Lrp2*$^{+/-}$;*Cdon*$^{+/-}$ mice were subjected to timed mating to collect embryos at the
466 depicted embryonic day. Neither *Cdon*$^{-/-}$ mice nor *Lrp2*$^{-/-}$ mice on the C57BL/6N display
467 anterior truncation phenotypes.
468

469 **Whole mount in situ hybridization**

470 Whole mount RNA in situ hybridization was performed according to standard protocols (Hong
471 and Krauss, 2012). Briefly, embryos were dissected out and fixed in 4% paraformaldehyde in
472 phosphate-buffered saline (PBS), dehydrated through a graded methanol series, and stored at -
473 20°C. Rehydrated embryos were treated with 10 μg/ml proteinase K (Qiagen) in PBS, 0.1%
474 Tween-20 (PBST) according to stage. Embryos were rinsed with PBST, post-fixed and
475 hybridized with digoxygenin (DIG)-labeled probe in hybridization mix (50% formamide, 1.3x SSC
476 pH 5.0, 5 mM EDTA, 50 μg/ml yeast tRNA, 100 μg/ml heparin, 0.2% Tween-20, and 0.5%
477 CHAPS) overnight at 65°C. They were washed, blocked with 2% Roche blocking reagent, 20%
478 heat-inactivated lamb serum in Tris-buffered saline with 0.1% Tween-20 (TBST) and incubated
479 with alkaline phosphate-conjugated anti-DIG antibody (1:2000, Roche) in blocking buffer
480 overnight at 4°C. After washing with TBST and NTMT (100 mM NaCl, 100 mM Tris pH9.5,
481 50mM $MgCl_2$, and 0.1% Tween-20), embryos were stained with BM Purple AP substrate
482 (Roche) in the dark. Stained embryos were cleared in 80% glycerol and photographed with a
483 Jenoptik ProgRes C3 camera attached to Nikon SMZ 1500 stereomicroscope. Captured images
484 were assembled by Helicon Focus software (Helicon Soft).
485

486 **Mouse epiblast stem cell culture and Western blot and qRT-PCR analysis**

487 Mouse epiblast stem cells (EpiSC9 cells) were obtained from Jianlong Wang and cultured as
488 described (Huang et al., 2017). Briefly, cells were cultured on 0.1% fibronectin-coated plates

489 (MilliporeSigma, 10 μg/ml/cm^2) in N2B27 media supplemented with 20 ng/ml Activin A (R&D
490 Systems) and 12 ng/ml Fgf2 (R&D Systems). Media were changed daily. EpiScs were treated
491 with EtOH for six hours in fresh EpiSC media with supplements. For protein analysis, cells were
492 harvested with RIPA buffer plus protease inhibitor (Sigma) and phosphatase inhibitor (Sigma).
493 Western blotting was as described (Bae et al., 2009). Images were scanned and quantified
494 using ImageJ software. Statistical significance was calculated using Student's t-test and a cutoff
495 of $p<0.05$. Primary antibodies used for Western blot: SMAD2 (Cell Signaling #5339), p-
496 SMAD2C (Cell Signaling #3108), p-SMAD2L (Cell Signaling #3104), JNK (Cell Signaling
497 #9252), p-JNK (Cell Signaling #9251), and GAPDH (Cell Signaling #97166). For mRNA
498 analysis, total RNA was extracted from EpiSCs using the RNAeasy kit (Quiagen). Reverse
499 transcription and cDNA production were performed with Superscript III first strand synthesis
500 system (Invitrogen). qPCR was performed using iQ SyBR green supermix (BioRad) on an
501 iCycler iQ5 (BioRad). Gene expression levels were normalized to *Gapdh*. qPCR primers are in
502 Supplemental Table 1.
503
504 **Protein-protein interactions**
505 Expression vectors encoding soluble, tagged forms of CDON, SHH-N, CD164, ActRIIA, ActRIIB,
506 ALK4, Cripto, and LRP2, and LRP2 mini-receptors that encoded the LRP2 transmembrane and
507 intracellular domains, were constructed by standard methods; details are available on request.
508 HEK293T (293T) cells were cultured in DMEM with 10% FBS and 1x Penicillin/Streptomycin.
509 293T cells in 10 cm dishes were transfected with a total of either 2 or 3 μg of plasmid vectors
510 using Effectene reagent (Qiagen). Media were changed to 2% FBS two days after transfection.
511 Conditioned media were harvested five days afterwards. Soluble fusion proteins in conditioned
512 media were quantified by dot blotting with human IgG Fc protein (Jackson ImmunoResearch
513 Laboratories) as a standard, and by alkaline phosphatase (AP) enzyme activity using AP yellow

514 liquid substrate (Sigma). For analysis of CDON-Fc interactions with soluble AP-tagged proteins,
515 the factors were coexpressed in HEK293T cells. For Fc pull down and AP activity assays with
516 CDON-Fc, soluble fusion proteins were incubated with protein G agarose beads (Roche) for 2
517 hours at 4°C. For analysis of soluble LRP2-Fc mini-receptors interactions with soluble AP-
518 tagged proteins, LRP2 sR1-sR4 and the AP-tagged counterparts were generated separately in
519 individual transfections and CM mixed together. Pull down complexes were washed five times
520 with ice-cold HNTG buffer (20 mM HEPES pH 7.5, 150mM NaCl, 0.1% Triton X-100, 10%
521 glycerol). Endogenous AP was inactivated by heat inactivation. AP activity in pull-down
522 complexes was measured using AP yellow liquid substrate (Sigma). For AP pull down followed
523 by Western blot analysis, soluble fusion proteins were incubated with anti-AP conjugated
524 agarose beads (Sigma) overnight at 4°C. Pull-down complexes were washed five times with
525 HNTG buffer, eluted from the beads by boiling, and separated by SDS-PAGE. Antibodies used
526 for Western blot were HRP conjugated with goat anti-human Fc.

527 To test SHH-N interaction with membrane-bound LRP2 mini-receptors, NIH3T3 cells
528 were transfected with the four individual LRP2 mini-receptors encoding transmembrane and
529 intracellular domains and incubated with 20μg/ml GST-SHH-N in the medium for two hours. Cell
530 lysates were immunoprecipitated with polyclonal LRP2 antibody directed against full-length
531 LRP2, and subjected to Western blot analysis with anti-LRP2 and anti-GST antibodies.

532

533

534

535 **Acknowledgements**

536 We thank Horoshi Hamada for providing *Lefty2* mutant mice and reagents; Michael Shen for
537 providing *Cripto* mutant mice and reagents; Zoe Fresquez and Marysia-Kolbe Rieder for
538 technical support; Xin Huang and Jianlong Wang for EpiSC9 cells and advice; Nadeera
539 Wickramasinghe and Nicole Dubois for generous support with cell culture; Steve Farber and
540 Phil Soriano for helpful discussions, and members of the Krauss lab for reading the manuscript.
541 This work was supported by NIH grant DE024748 from the National Institute of Dental and
542 Craniofacial Research to R.S.K. and German Research Foundation grant CH1838/1-1 to A.
543 Christ.

544

545 **Competing interests**

546 The authors declare no competing interests.

547 **References**

548 Abe, Y., Kruszka, P., Martinez, A.F., Roessler, E., Shiota, K., Yamada, S., and Muenke, M.
549 (2018). Clinical and Demographic Evaluation of a Holoprosencephaly Cohort From the Kyoto
550 Collection of Human Embryos. Anat Rec *301*, 973-986.
551
552 Allen, B.L., Song, J.Y., Izzi, L., Althaus, I.W., Kang, J.-S., Charron, F., R.S. Krauss, R.S., and
553 McMahon, A.P. (2011). Overlapping roles and collective requirement for the co-receptors Gas1,
554 Cdo and Boc in Shh pathway function. Dev Cell *20*, 775-787.
555
556 Andersson, O., Reissmann, E., Jörnvall, H., and Ibáñez, C.F. (2006). Synergistic interaction
557 between Gdf1 and Nodal during anterior axis development. Dev Biol *293*, 370-381.
558
559 Ang, S.L., and Rossant, J. (1994). HNF-3β is essential for node and notochord formation in
560 mouse development. Cell *78*, 561-574.
561
562 Aoto, K., Shikata, Y., Higashiyama, D., Shiota, K., and Motoyama, J. (2008). Fetal ethanol
563 exposure activates protein kinase A and impairs Shh expression in prechordal mesendoderm
564 cells in the pathogenesis of holoprosencephaly. Birth Defects Res A Clin Mol Teratol *82*, 224-
565 231.
566
567 Aoto, K., Shikata, Y., Imai, H., Matsumaru, D., Tokunaga, T., Shioda, S., Yamada, G., and
568 Motoyama, J. (2009). Mouse Shh is required for prechordal plate maintenance during brain and
569 craniofacial morphogenesis. Dev Biol *327*, 106-120.
570
571 Bae, G.U., Domené, S., Roessler, E., Schachter, K., Kang, J.S., Muenke, M., and Krauss, R.S.
572 (2011). Mutations in CDON, Encoding a Hedgehog Receptor, Result in Holoprosencephaly and
573 Defective Interactions with Other Hedgehog Receptors. Am J Hum Genet *89*, 231-240.
574
575 Bae, G.U., Yang, Y.J., Jiang, G., Hong, M., Lee, H.J., Tessier-Lavigne, M., Kang, J.S., and
576 Krauss, R.S. (2009). Neogenin regulates skeletal myofiber size and focal adhesion kinase and
577 extracellular signal-regulated kinase activities in vivo and in vitro. Mol Biol Cell *20*, 4920-4931.
578
579 Barone, V., Lang, M., Krens, S.F.G., Pradhan, S.J., Shamipour, S., Sako, K., Sikora, M., Guet,
580 C.C., and Heisenberg, C.-P. (2017). An Effective Feedback Loop between Cell-Cell Contact
581 Duration and Morphogen Signaling Determines Cell Fate. Dev Cell *43*, 198-211.e112.
582
583 Beachy, P.A., Hymowitz, S.G., Lazarus, R.A., Leahy, D.J., and Siebold, C. (2010). Interactions
584 between Hedgehog proteins and their binding partners come into view. Genes Dev *15*, 2001-
585 2012.
586
587 Belo, J.A., Leyns, L., Yamada, G., and De Robertis, E.M. (1998). The prechordal midline of the
588 chondrocranium is defective in Goosecoid-1 mouse mutants. Mech Dev *72*, 15-25.
589
590 Brons, I.G.M., Smithers, L.E., Trotter, M.W.B., Rugg-Gunn, P., Sun, B., Chuva de Sousa Lopes,
591 S.M., Howlett, S.K., Clarkson, A., Ahrlund-Richter, L., Pedersen, R.A.*, et al.* (2007). Derivation
592 of pluripotent epiblast stem cells from mammalian embryos. Nature *448*, 191-195.
593
594 Chng, Z., Teo, A., Pedersen, R.A., and Vallier, L. (2010). SIP1 Mediates Cell-Fate Decisions
595 between Neuroectoderm and Mesendoderm in Human Pluripotent Stem Cells. Cell Stem Cell *6*,
596 59-70.

597
598 Christ, A., Christa, A., Kur, E., Lioubinski, O., Bachmann, S., Willnow, T.E., and Hammes, A.
599 (2012). LRP2 Is an Auxiliary SHH Receptor Required to Condition the Forebrain Ventral Midline
600 for Inductive Signals. Developmental Cell *22*, 268-278.
601
602 Chu, J., Ding, J., Jeays-Ward, K., Price, S.M., Placzek, M., and Shen, M.M. (2005). Non-cell-
603 autonomous role for Cripto in axial midline formation during vertebrate embryogenesis.
604 Development *132*, 5539-5551.
605
606 Cohen, M.M., Jr. (2006). Holoprosencephaly: clinical, anatomic, and molecular dimensions.
607 Birth Defects Res Part A Clin Mol Teratol *76*, 658-673.
608
609 Cohen, M.M., Jr. , and Shiota, K. (2002). Teratogenesis of holoprosencephaly. Am J Med Genet
610 *109*, 1-15.
611
612 Cole, F., and Krauss, R.S. (2003). Microform holoprosencephaly in mice that lack the Ig
613 superfamily member Cdon. Curr Biol *13*, 411-415.
614
615 Constam, D.B. (2009). Riding Shotgun: A Dual Role for the Epidermal Growth Factor-
616 Cripto/FRL-1/Cryptic Protein Cripto in Nodal Trafficking. Traffic *10*, 783-791.
617
618 Cordero, D., Marcucio, R., Hu, D., Gaffield, W., Tapadia, M., and Helms, J.A. (2004). Temporal
619 perturbations in sonic hedgehog signaling elicit the spectrum of holoprosencephaly phenotypes.
620 J Clin Invest *114*, 485-494.
621
622 Croen, L.A., Shaw, G.M., and Lammer, E.J. (2000). Risk factors for cytogenetically normal
623 holoprosencephaly in California: a population-based case-control study. Am J Med Genet *90*,
624 320-325.
625
626 Croy, J.E., Shin, W.D., Knauer, M.F., Knauer, D.J., and Komives, E.A. (2003). All Three LDL
627 Receptor Homology Regions of the LDL Receptor-Related Protein Bind Multiple Ligands.
628 Biochemistry *42*, 13049-13057.
629
630 Ding, J., Yang, L., Yan, Y.T., Chen, A., Desai, N., Wynshaw-Boris, A., and Shen, M.M. (1998).
631 Cripto is required for correct orientation of the anterior-posterior axis in the mouse embryo.
632 Nature *395*, 702-707.
633
634 Dubourg, C., Kim, A., Watrin, E., de Tayrac, M., Odent, S., David, V., and Dupé, V. (2018).
635 Recent advances in understanding inheritance of holoprosencephaly. Am J Med Genet *178*,
636 258-269.
637
638 Echelard, Y., Epstein, D.J., St-Jacques, B., Shen, L., Mohler, J., McMahon, J.A., and McMahon,
639 A.P. (1993). Sonic hedgehog, a member of a family of putative signaling molecules, is
640 implicated in the regulation of CNS polarity. Cell *75*, 1417-1430.
641
642 Filosa, S., Rivera-Pérez, J.A., Gómez, A.P., Gansmuller, A., Sasaki, H., Behringer, R.R., and
643 Ang, S.L. (1997). Goosecoid and HNF-3β genetically interact to regulate neural tube patterning
644 during mouse embryogenesis. Development *124*, 2843-2854.
645
646 Geng, X., and Oliver, G. (2009). Pathogenesis of holoprosencephaly. J Clin Invest *119*, 1403-
647 1413.

648
649 Grimm, O.H., and Gurdon, J.B. (2002). Nuclear exclusion of Smad2 is a mechanism leading to
650 loss of competence. Nat Cell Biol *4*, 519-522.
651
652 Heyne, G.W., Melberg, C.G., Doroodchi, P., Parins, K.F., Kietzman, H.W., Everson, J.L., Ansen-
653 Wilson, L.J., and Lipinski, R.J. (2015). Definition of Critical Periods for Hedgehog Pathway
654 Antagonist-Induced Holoprosencephaly, Cleft Lip, and Cleft Palate. PLOS ONE *10*, e0120517.
655
656 Hong, M., and Krauss, R.S. (2012). *Cdon* mutation and fetal ethanol exposure synergize to
657 produce midline signaling defects and holoprosencephaly spectrum disorders in mice PLOS
658 Genet *8*, e1002999.
659
660 Hong, M., and Krauss, R.S. (2013). Rescue of Holoprosencephaly in Fetal Alcohol-Exposed
661 Cdon Mutant Mice by Reduced Gene Dosage of Ptch1. PLOS ONE *8*, e79269.
662
663 Hong, M., and Krauss, R.S. (2017). Ethanol itself is a holoprosencephaly-inducing teratogen.
664 PLOS ONE *12*, e0176440.
665
666 Hong, M., and Krauss, R.S. (2018). Modeling the complex etiology of holoprosencephaly in
667 mice. Am J Med Genet C *178*, 140-150.
668
669 Huang, X., Balmer, S., Yang, F., Fidalgo, M., Li, D., Guallar, D., Hadjantonakis, A.K., and Wang,
670 J. (2017). Zfp281 is essential for mouse epiblast maturation through transcriptional and
671 epigenetic control of Nodal signaling. eLife *6*, e33333.
672
673 Izzi, L., Lévesque, M., Morin, S., Laniel, D., Wilkes, B.C., Mille, F., Krauss, R.S., McMahon,
674 A.P., Allen, B.L., and Charron, F. (2011). Boc and Gas1 each form distinct Shh receptor
675 complexes with Ptch1 and are required for Shh-mediated cell proliferation. Dev Cell *20*, 788-
676 801.
677
678 Jeong, M.-H., Ho, S.-M., Vuong, T.A., Jo, S.-B., Liu, G., Aaronson, S.A., Leem, Y.-E., and Kang,
679 J.-S. (2014). Cdo suppresses canonical Wnt signalling via interaction with Lrp6 thereby
680 promoting neuronal differentiation. Nat Commun *5*, 5455.
681
682 Johnson, C.Y., and Rasmussen, S.A. (2010). Non-genetic risk factors for holoprosencephaly.
683 Am J Med Genet C Semin Med Genet *154C*, 73-85.
684
685 Kang, J.-S., Feinleib, J.L., Knox, S., Ketteringham, M.A., and Krauss, R.S. (2003). Promyogenic
686 members of the Ig and cadherin families associate to positively regulate differentiation. Proc
687 Natl Acad Sci (USA) *100*, 3989-3994.
688
689 Kang, J.-S., Mulieri, P.J., Hu, Y., Taliana, L., and Krauss, R.S. (2002). BOC, an Ig superfamily
690 member, associates with CDO to positively regulate myogenic differentiation. EMBO J *21*, 114-
691 124.
692
693 Kang, J.-S., Yi, M.-J., Zhang, W., Feinleib, J.L., Cole, F., and Krauss, R.S. (2004). Netrins and
694 neogenin promote myotube formation. J Cell Biol *167*, 493-504.
695
696 Kiecker, C., and Niehrs, C. (2001). The role of prechordal mesendoderm in neural patterning.
697 Curr Opin Neurobiol *11*, 27-33.
698

699 Kietzman, H.W., Everson, J.L., Sulik, K.K., and Lipinski, R.J. (2014). The Teratogenic Effects of
700 Prenatal Ethanol Exposure Are Exacerbated by Sonic Hedgehog or Gli2 Haploinsufficiency in
701 the Mouse. PLOS ONE *9*, e89448.
702
703 Kojima, Y., Kaufman-Francis, K., Studdert, J.B., Steiner, K.A., Power, M.D., Loebel, D.A.F.,
704 Jones, V., Hor, A., de Alencastro, G., Logan, G.J.*, et al.* (2014). The Transcriptional and
705 Functional Properties of Mouse Epiblast Stem Cells Resemble the Anterior Primitive Streak.
706 Cell Stem Cell *14*, 107-120.
707
708 Kong, J.H., Siebold, C., and Rohatgi, R. (2019). Biochemical mechanisms of vertebrate
709 hedgehog signaling. Development *146*, dev166892.
710
711 Krauss, R.S. (2007). Holoprosencephaly: new models, new insights. Expert Rev Mol Med *9*, 1-
712 17.
713
714 Krauss, R.S., and Hong, M. (2016). Gene–Environment Interactions and the Etiology of Birth
715 Defects. Curr Top Dev Biol *116*, 569-580.
716
717 Kretzschmar, M., Doody, J., Timokhina, I., and Massagué, J. (1999). A mechanism of
718 repression of TGFβ/ Smad signaling by oncogenic Ras. Genes Dev *13*, 804-816.
719
720 Lacbawan, F., Solomon, B.D., Roessler, E., El-Jaick, K., Domené, S., Vélez, J.I., Zhou, N.,
721 Hadley, D., Balog, J.Z., Long, R.*, et al.* (2009). Clinical spectrum of SIX3-associated mutations
722 in holoprosencephaly: correlation between genotype, phenotype and function. J Med Genet *46*,
723 389-398.
724
725 Lee, R.T.H., Zhao, Z., and Ingham, P.W. (2016). Hedgehog signalling. Development *143*, 367-
726 372.
727
728 Leoncini, E., Baranello, G., Orioli, I.M., Annerén, G., Bakker, M., Bianchi, F., Bower, C.,
729 Canfield, M.A., Castilla, E.E., Cocchi, G.*, et al.* (2008). Frequency of holoprosencephaly in the
730 International Clearinghouse Birth Defects Surveillance Systems: searching for population
731 variations. Birth Defects Res A Clin Mol Teratol *82*, 585-591.
732
733 Lessard, S.J., MacDonald, T.L., Pathak, P., Han, M.S., Coffey, V.G., Edge, J., Rivas, D.A.,
734 Hirshman, M.F., Davis, R.J., and Goodyear, L.J. (2018). JNK regulates muscle remodeling via
735 myostatin/SMAD inhibition. Nat Commun *9*, 3030.
736
737 Li, L., Song, L., Liu, C., Chen, J., Peng, G., Wang, R., Liu, P., Tang, K., Rossant, J., and Jing,
738 N. (2015). Ectodermal progenitors derived from epiblast stem cells by inhibition of Nodal
739 signaling. J Mol Cell Biol *7*, 455-465.
740
741 Liu, C., Wang, R., He, Z., Osteil, P., Wilkie, E., Yang, X., Chen, J., Cui, G., Guo, W.e., Chen, Y.*,*
742 *et al.* (2018). Suppressing Nodal Signaling Activity Predisposes Ectodermal Differentiation of
743 Epiblast Stem Cells. Stem Cell Reports *11*, 43-57.
744
745 Lowe, L.A., Yamada, S., and Kuehn, M.R. (2001). Genetic dissection of nodal function in
746 patterning the mouse embryo. Development *128*, 1831-1843.
747

Lu, M., and Krauss, R.S. (2010). N-cadherin ligation, but not Sonic hedgehog binding, initiates Cdo-dependent p38α/β MAPK signaling in skeletal myoblasts. Proc Natl Acad Sci (USA) *107*, 4212-4217.

Lyon, R.C., McComb, J.A., Schreurs, J., and Goldstein, D.B. (1981). A relationship between alcohol intoxication and the disordering of brain membranes by a series of short-chain alcohols. J Pharmacol Exp Ther *218*, 669-675.

Marcucio, R.S., Young, N.M., Hu, D., and Hallgrimsson, B. (2011). Mechanisms that underlie co-variation of the brain and face. Genesis *49*, 177-189.

Massagué, J. (2003). Integration of Smad and MAPK pathways: a link and a linker revisited. Genes Dev *17*, 2993-2997.

McAlhany, R.E., West, J.R., and Miranda, R.C. (2000). Glial-derived neurotrophic factor (GDNF) prevents ethanol-induced apoptosis and JUN kinase phosphorylation. Dev Brain Res *119*, 209-216.

McCarns, S.C., Hansch, C., Caldwell, W.S., Morgan, W.T., Moore, S.K., and Doolittle, D.J. (1997). Correlation between hydrophobicity of short-chain aliphatic alcohols and their ability to alter plasma membrane integrity. Fundam Appl Toxicol *36*, 62-70.

McCarthy, N., Wetherill, L., Lovely, C.B., Swartz, M.E., Foroud, T.M., and Eberhart, J.K. (2013). Pdgfra protects against ethanol-induced craniofacial defects in a zebrafish model of FASD. Development *140*, 3254-3265.

McCarthy, R.A., Barth, J.L., Chintalapudi, M.R., Knaak, C., and Argraves, W.S. (2002). Megalin functions as an endocytic sonic hedgehog receptor. J Biol Chem *277*, 25660-25667.

McMahon, A.P., Ingham, P.W., and Tabin, C.J. (2003). Developmental roles and clinical significance of hedgehog signaling. Curr Top Dev Biol *53*, 1-114.

Meno, C., Gritsman, K., Ohishi, S., Ohfuji, Y., Heckscher, E., Mochida, K., Shimono, A., Kondoh, H., Talbot, W.S., Robertson, E.J.*, et al.* (1999). Mouse Lefty2 and Zebrafish Antivin Are Feedback Inhibitors of Nodal Signaling during Vertebrate Gastrulation. Mol Cell *4*, 287-298.

Miller, E.A., Rasmussen, S.A., Siega-Riz, A.M., Frías, J.L., Honein, M.A., and Study., N.B.D.P. (2010). Risk factors for non-syndromic holoprosencephaly in the National Birth Defects Prevention Study. Am J Med Genet C Semin Med Genet *154C*, 62-72.

Muenke, M., and Beachy, P.A. (2001). Holoprosencephaly. In The Metabolic & Molecular Bases of Inherited Disease, C.R. Scriver, A.L. Beaudet, W.S. Sly, and D. Valle, eds. (New York: McGraw-Hill), pp. 6203-6230.

Mulieri, P.J., Okada, A., Sassoon, D.A., McConnell, S.K., and Krauss, R.S. (2000). Developmental expression pattern of the *cdo* gene. Dev Dyn *219*, 40-49.

Mulieri, P.M., Kang, J.-S., Sassoon, D.A., and Krauss, R.S. (2002). Expression of the *boc* gene during murine embryogenesis. Dev Dyn *223*, 379-388.

Najm, F.J., Chenoweth, J.G., Anderson, P.D., Nadeau, J.H., Redline, R.W., McKay, R.D.G., and Tesar, P.J. (2011). Isolation of Epiblast Stem Cells from Preimplantation Mouse Embryos. Cell Stem Cell *8*, 318-325.

Nomura, M., and Li, E. (1998). Smad2 role in mesoderm formation, left-right patterning and craniofacial development. Nature *393*, 786-790.

Pauklin, S., and Vallier, L. (2015). Activin/Nodal signalling in stem cells. Development *142*, 607-619.

Petrov, K., Wierbowski, B.M., and Salic, A. (2017). Sending and Receiving Hedgehog Signals. Annu Rev Cell Dev Biol *33*, 145-168.

Powell, D.R., Williams, J.S., Hernandez-Lagunas, L., Salcedo, E., O'Brien, J.H., and Artinger, K.B. (2015). Cdon promotes neural crest migration by regulating N-cadherin localization. Dev Biol *407*, 289-299.

Ren, Z., Wang, X., Yang, F., Xu, M., Frank, J.A., Wang, H., Wang, S., Ke, Z., and Luo, J. (2017). Ethanol-induced damage to the developing spinal cord: The involvement of CCR2 signaling. Biochim Biophys Acta Mol Basis Dis *1863*, 2746-2761.

Rezaei, H.B., Kamato, D., Ansari, G., Osman, N., and Little, P.J. (2012). Cell biology of Smad2/3 linker region phosphorylation in vascular smooth muscle. Clin Exp Pharmacol Physiol *39*, 661-667.

Robertson, E.J. (2014). Dose-dependent Nodal/Smad signals pattern the early mouse embryo. Semin Cell Dev Biol *32*, 73-79.

Roessler, E., Hu, P., Marino, J., Hong, S., Hart, R., Berger, S., Martinez, A., Abe, Y., Kruszka, P., Thomas, J.W.*, et al.* (2018a). Common genetic causes of holoprosencephaly are limited to a small set of evolutionarily conserved driver genes of midline development coordinated by TGF-β, hedgehog, and FGF signaling. Hum Mutat *39*, 1416-1427.

Roessler, E., Hu, P., and Muenke, M. (2018b). Holoprosencephaly in the genomics era. Am J Med Genet C *178*, 165-174.

Roessler, E., Vélez, J.I., Zhou, N., and Muenke, M. (2012). Utilizing prospective sequence analysis of SHH, ZIC2, SIX3 and TGIF in holoprosencephaly probands to describe the parameters limiting the observed frequency of mutant gene×gene interactions. Mol Genet Metab *105*, 658-664.

Rubenstein, J.L., and Beachy, P.A. (1998). Patterning of the embryonic forebrain. Curr Opin Neurobiol *8*, 18-26.

Sanchez-Arrones, L., Cardozo, M., Nieto-Lopez, F., and Bovolenta, P. (2012). Cdon and Boc: Two transmembrane proteins implicated in cell–cell communication. Int J Biochem Cell Biol *44*, 698-702.

Schier, A.F. (2009). Nodal morphogens. Cold Spring Harb Perspect Biol *1*, a003459.

Shen, M.M. (2007). Nodal signaling: developmental roles and regulation. Development *134*, 1023-1034.

Shiota, K., and Yamada, S. (2010). Early pathogenesis of holoprosencephaly. Am J Med Genet C Semin Med Genet *154C*, 22-28.

Solomon, B., Bear, K., Wyllie, A., Keaton, A., Dubourg, C., David, V., Mercier, S., Odent, S., Hehr, U., Paulussen, A.*, et al.* (2012). Genotypic and phenotypic analysis of 396 individuals with mutations in Sonic Hedgehog. J Med Genet *49*, 473-479.

Solomon, B.D., Mercier, S., Vélez, J.I., Pineda-Alvarez, D.E., Wyllie, A., Zhou, N., Dubourg, C., David, V., Odent, S., Roessler, E.*, et al.* (2010). Analysis of genotype-phenotype correlations in human holoprosencephaly. Am J Med Genet C Semin Med Genet *154C*, 133-141.

Song, J., Oh, S.P., Schrewe, H., Nomura, M., Lei, H., Okano, M., Gridley, T., and Li, E. (1999). The type II activin receptors are essential for egg cylinder growth, gastrulation, and rostral head development in mice. Dev Biol *213*, 157-169.

Sparrow, D.B., Chapman, G., Smith, A.J., Mattar, M.Z., Major, J.A., O'Reilly, V.C., Saga, Y., Zackai, E.H., Dormans, J.P., Alman, B.A.*, et al.* (2012). A mechanism for gene-environment interaction in the etiology of congenital scoliosis. Cell *149*, 295-306.

Spoelgen, R., Hammes, A., Anzenberger, U., Zechner, D., Andersen, O.M., Jerchow, B., and Willnow, T.E. (2005). LRP2/megalin is required for patterning of the ventral telencephalon. Development *132*, 405-414.

Sulik, K.K., Johnston, M.C., and Webb, M.A. (1981). Fetal alcohol syndrome: embryogenesis in a mouse model. Science *214*, 936-938.

Summers, A.D., Reefhuis, J., Taliano, J., and Rasmussen, S.A. (2018). Nongenetic risk factors for holoprosencephaly: An updated review of the epidemiologic literature. Am J Med Genet C *178*, 151-164.

Tenzen, T., Allen, B.L., Cole, F., Kang, J.-S., Krauss, R.S., and McMahon, A.P. (2006). The cell surface membrane proteins Cdo and Boc are components and targets of the hedgehog signaling pathway and feedback network in mice. Dev Cell *10*, 647-656.

Tsakiridis, A., Huang, Y., Blin, G., Skylaki, S., Wymeersch, F., Osorno, R., Economou, C., Karagianni, E., Zhao, S., Lowell, S.*, et al.* (2014). Distinct Wnt-driven primitive streak-like populations reflect in vivo lineage precursors. Development *141*, 1209-1221.

Vallier, L., Mendjan, S., Brown, S., Chng, Z., Teo, A., Smithers, L.E., Trotter, M.W.B., Cho, C.H.-H., Martinez, A., Rugg-Gunn, P.*, et al.* (2009). Activin/Nodal signalling maintains pluripotency by controlling Nanog expression. Development *136*, 1339-1349.

Willnow, T.E., and Christ, A. (2017). Endocytic receptor LRP2/megalin—of holoprosencephaly and renal Fanconi syndrome. Pflügers Archiv *469*, 907-916.

Willnow, T.E., Christ, A., and Hammes, A. (2012). Endocytic receptor-mediated control of morphogen signaling. Development *139*, 4311-4319.

Willnow, T.E., Hilpert, J., Armstrong, S.A., Rohlmann, A., Hammer, R.E., Burns, D.K., and Herz, J. (1996). Defective forebrain development in mice lacking gp330/megalin. Proc Natl Acad Sci (USA) *93*, 8460-8464.

Zalc, A., Rattenbach, R., Auradé, F., Cadot, B., and Relaix, F. (2015). Pax3 and Pax7 Play Essential Safeguard Functions against Environmental Stress-Induced Birth Defects. Dev Cell *33*, 56-66.

Zhang, W., Kang, J.-S., Cole, F., Yi, M.J., and Krauss, R.S. (2006). Cdo functions at multiple points in the Sonic Hedgehog pathway, and Cdo-deficient mice accurately model human holoprosencephaly. Dev Cell *10*, 657-665.

Zhang, X.M., Ramalho-Santos, M., and McMahon, A.P. (2001). Smoothened mutants reveal redundant roles for Shh and Ihh signaling including regulation of L/R symmetry by the mouse node. Cell *106*, 781-792.

Zheng, X., Mann, R.K., Sever, N., and Beachy, P.A. (2010). Genetic and biochemical definition of the Hedgehog receptor. Genes Dev *24*, 57-71.

919 **Table 1: Time course of EtOH-Induced HPE in *Cdon*$^{-/-}$ Embryos**

920

EtOH treatment:	**E7.25**				**E7.5**	
	Saline		EtOH		EtOH	
Phenotype*	*Cdon*$^{+/-}$	*Cdon*$^{-/-}$	*Cdon*$^{+/-}$	*Cdon*$^{-/-}$	*Cdon*$^{+/-}$	*Cdon*$^{-/-}$
Fused upper lip	0/17	2/14	0/21	13/24**	0/13	0/22
Single nostril	0/17	0/14	0/21	5/24	0/13	0/22
Proboscis	0/17	0/14	0/21	2/24	0/13	0/22

* All embryos with HPE had fused upper lip, a fraction of these showed single nostril and proboscis.

**p=0.0165 by Fisher's two-tailed exact test, when compared to EtOH-treated *Cdon*$^{+/-}$ embryos.

921

922

923

924

925

926

927

928 **Table 2: *Cripto* Heterozygosity Enhances EtOH-Induced HPE in *Cdon*$^{-/-}$ Embryos**

Treatment	Genotype (# embryos with HPE/total (%))*		
	Cdon$^{+/-}$;*Cripto*$^{+/-}$	*Cdon*$^{-/-}$;*Cripto*$^{+/+}$	*Cdon*$^{-/-}$;*Cripto*$^{+/-}$
Saline	0/23 (0%)	0/11 (0%)	2/27 (7.4%)
EtOH (2.9 g/kg)	1/48 (2.1%)	9/32 (28.1%)	31/56 (55.4%)**

929

* Crosses between the following genotypes were used to generate the genotypes scored above:

Cdon$^{+/-}$;*Cripto*$^{+/-}$ x *Cdon*$^{+/-}$;*Cripto*$^{+/-}$

Cdon$^{+/-}$;*Cripto*$^{+/-}$ x *Cdo-*$^{+/-}$;*Cripto*$^{+/-}$

Cdon$^{+/-}$ x *Cdon*$^{+/-}$;*Cripto*$^{+/-}$

Cdon$^{+/-}$ x *Cdon*$^{-/-}$;*Cripto*$^{+/-}$

Cdon$^{-/-}$ x *Cdon*$^{+/-}$;*Cripto*$^{+/-}$

No HPE was found in offspring genotypes other than those shown.

** p=0.014 by Fisher's two-tailed exact test, when compared to EtOH-treated *Cdon*$^{-/-}$;*Cripto*$^{+/+}$ embryos.

930

931

932

933

934

935

936

937

938

939

940 **Table 3: *Lefty2* Heterozygosity Supresses EtOH-Induced HPE in *Cdon*$^{-/-}$ Embryos**

Treatment	Genotype (# affected/total (%))*			
	Total HPE		Single nostril	
	Cdon$^{-/-}$;*Lefty2*$^{+/+}$	*Cdon*$^{-/-}$;*Lefty2*$^{+/-}$	*Cdon*$^{-/-}$;*Lefty2*$^{+/+}$	*Cdon*$^{-/-}$;*Lefty2*$^{+/-}$
Saline	1/12 (8.3%)	0/10 (0%)	0/12 (0%)	0/10 (0%)
EtOH (3.48 g/kg)	33/47 (70.2%)	26/48 (54.2%)	10/47 (21.3%)	3/48 (6.3%)**

941

* Crosses between the following genotypes were used to generate the genotypes scored above:

Cdon$^{+/-}$;*Lefty2*$^{+/-}$ x *Cdon*$^{+/-}$;*Lefty2*$^{+/-}$

Cdon$^{+/-}$;*Lefty2*$^{+/-}$ x *Cdo-*$^{+/-}$;*Lefty2*$^{+/-}$

Cdon$^{+/-}$ x *Cdon*$^{+/-}$;*Lefty2*$^{+/-}$

Cdon$^{+/-}$ x *Cdo*$^{-/-}$;*Lefty2*$^{+/-}$

Cdon$^{-/-}$ x *Cdon*$^{+/-}$;*Lefty2*$^{+/-}$

No HPE was found in offspring genotypes other than those shown.

** p=0.04 by Fisher's two-tailed exact test, when compared to EtOH-treated *Cdon*$^{-/-}$;*Lefty2*$^{+/+}$ embryos with a single nostril.

942

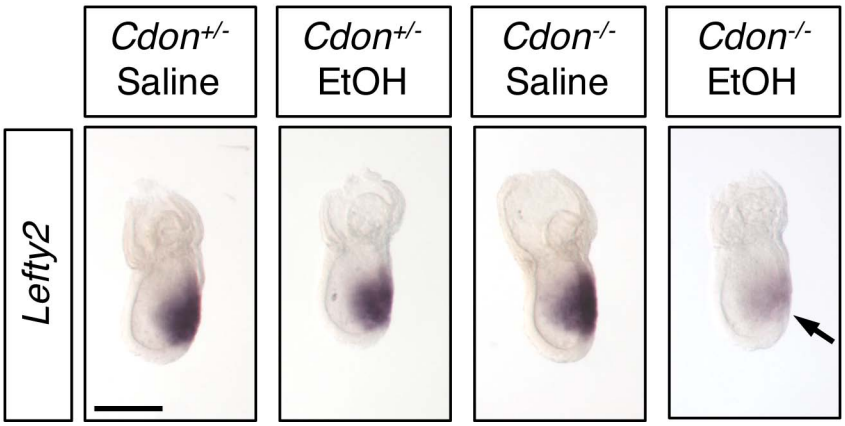

Figure 1. Defective Expression of *Lefty2* at the Primitive Streak Stage of EtOH-Treated *Cdon*$^{-/-}$ Embryos

Whole mount in situ hybridization analyses of *Lefty2* in embryos of the indicated genotype and treatment harvested at E7.25. *Lefty2* expression was decreased specifically in EtOH-treated *Cdon*$^{-/-}$ embryos. Numbers of embryos with similar results: *Cdon*$^{+/-}$ (saline) = 6; *Cdon*$^{+/-}$ (EtOH) = 4; *Cdon*$^{-/-}$ (saline) = 9; *Cdon*$^{-/-}$ (EtOH) = 9. Scale Bar, 200 μm.

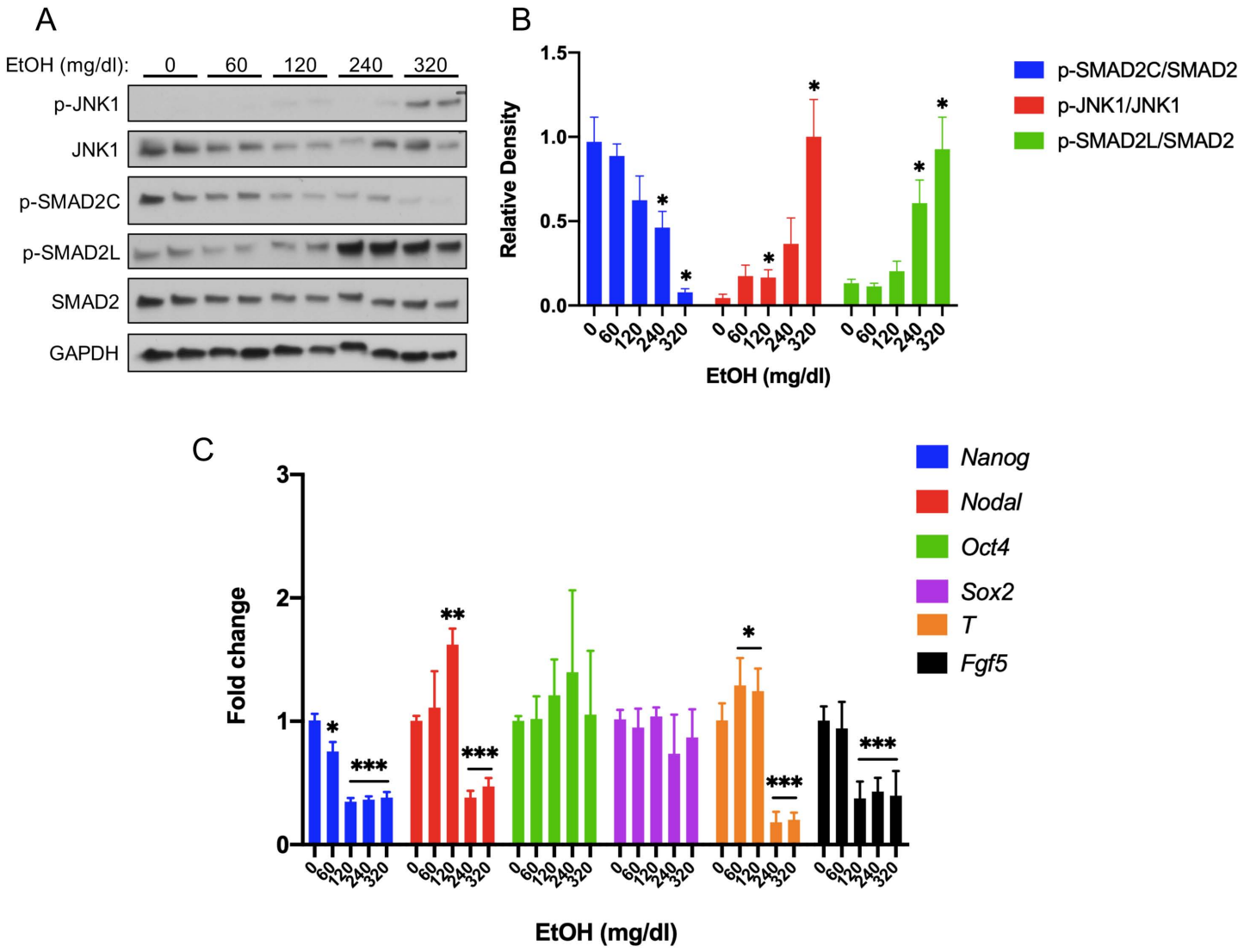

Figure 2: Acute EtOH Treatment Diminishes p-SMAD2C Levels and Enhances p-JNK1 and p-SMAD2L Levels in mEpiSCs

(A) Representative Western blot of mEpiSCs treated with the indicated doses of EtOH for 6 hours. GAPDH was used as a loading control. (B) Densitometric quantification of p-SMAD2C levels, relative to total Smad2; p-JNK1 levels, relative to total JNK1; and p-SMAD2L levels, relative to total SMAD2, with the indicated doses of EtOH. N=3 experiments with two biological replicates (as shown in (A)) in each experiment. (C) qRT-PCR analysis of *Nanog*, *Nodal*, *Oct4*, and *Sox2* expression in mEpiSCs treated with the indicated doses of EtOH for 6 hours. Expression was normalized to *Gapdh* expression. N=3 experiments with two biological replicates in each experiment. Values for (B) and (C) are means ± SEM, *p<0.05, **p<0.01, ***p,0.001.

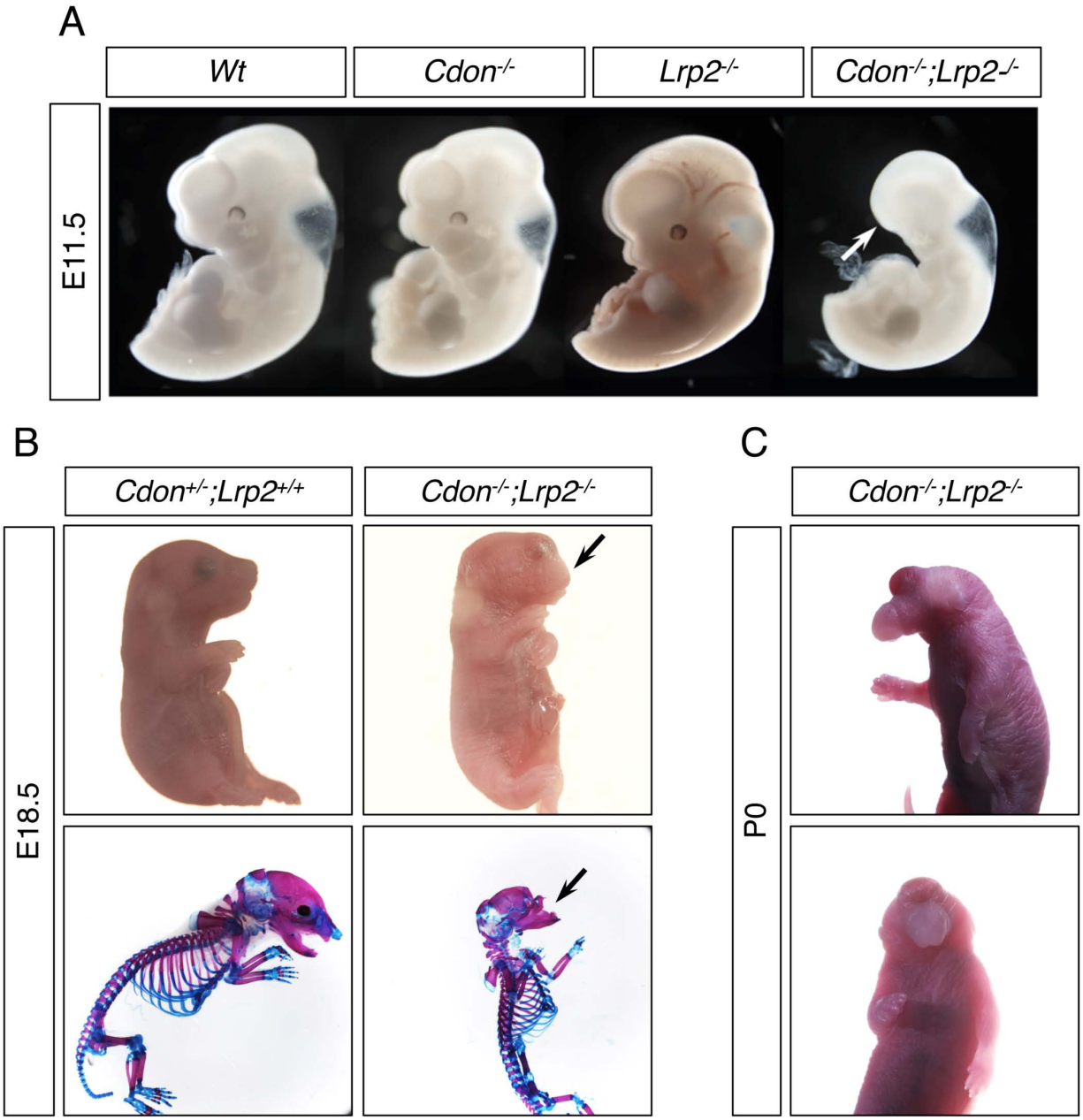

Figure 3: *Cdon* and *Lrp2* Interact Genetically to Produce HPE and Anterior Truncations in Mice

(A) Whole mount E11.5 embryos of the indicated genotype. Note the loss of anterior head structures in the *Cdon*$^{-/-}$;*Lrp2*$^{-/-}$ embryo (arrow). (B) E18.5 embryos of the indicated genotype in whole mount and alizarin red/alcian blue-stained skeleton preparations. Note the craniofacial truncation in the *Cdon*$^{-/-}$;*Lrp2*$^{-/-}$ embryos (arrows). (C) Whole mount P0 *Cdon*$^{-/-}$;*Lrp2*$^{-/-}$ embryo showing severe HPE.

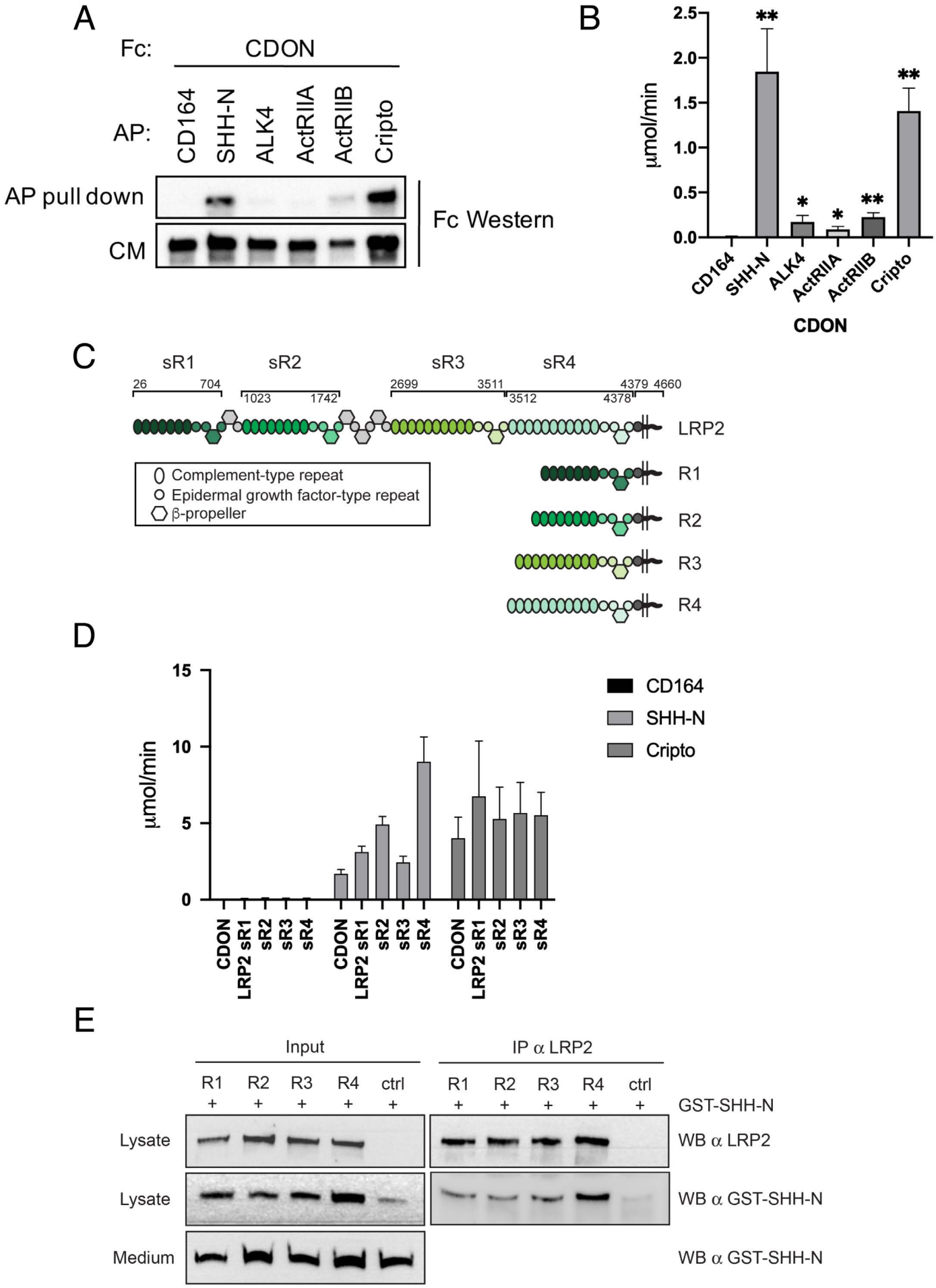
A
Fc:
CDON
AP:
CD164
SHH-N
ALK4
ActRIIA
ActRIIB
Cripto
AP pull down
CM
Fc Western
B
μmol/min
2.5
2.0
1.5
1.0
0.5
0.0
**
*
*
**
**
CD164
SHH-N
ALK4
ActRIIA
ActRIIB
Cripto
CDON
C
sR1
sR2
sR3
sR4
26
704
1023
1742
2699
3511
3512
4378
4379
4660
LRP2
Complement-type repeat
Epidermal growth factor-type repeat
β-propeller
R1
R2
R3
R4
D
μmol/min
15
10
5
0
CD164
SHH-N
Cripto
CDON
LRP2
sR1
sR2
sR3
sR4
E
Input
IP α LRP2
R1
R2
R3
R4
ctrl
GST-SHH-N
Lysate
Lysate
Medium
WB α LRP2
WB α GST-SHH-N
WB α GST-SHH-N

Figure 4: CDON and LRP2 Bind to Cripto

(A) The indicated AP-tagged proteins were co-expressed with CDON-Fc, and equivalent amounts of AP proteins in conditioned medium (CM) were pulled down. Levels of CDON-Fc in CM and in the pull down were detected by Western blot. (B) CDON-Fc was pulled down from CM derived from transfections as in (A), the amount of CDON-Fc from various CM normalized, and associated AP enzyme activity quantified. N=3, repeated four times for (A) and (B). (C) Schematic of full length LRP2 and recombinant mini-receptor variants used. Each mini-receptor spans one of the four repetitive modules of the extracellular receptor domain and was expressed either as soluble ectodomain fragments fused to IgG Fc (designated sR1- sR4) or as a membrane-bound mini-receptor fused to the authentic transmembrane and intracellular domains of LRP2 (designated R1- R4). Soluble ectodomain fragments sR1 – sR4 were studied in panel (D), whereas mini-receptors R1 – R4 were used in panel (E). Amino acid numbers next to the full length receptor polypeptide indicate the extent of individual receptor domains. (D) The indicated Fc-tagged proteins were pulled down from CM derived from transfections as in (A), the amount of Fc-tagged protein from various CM normalized, and associated AP enzyme activity quantified. N=3, repeated four times. (E) Cell transfectants expressing the indicated Lrp2 mini-receptor were incubated with GST-SHH-N, and cell lysates immunoprecipitated with antibody to LRP2 and blotted with antibodies to LRP2 and GST.

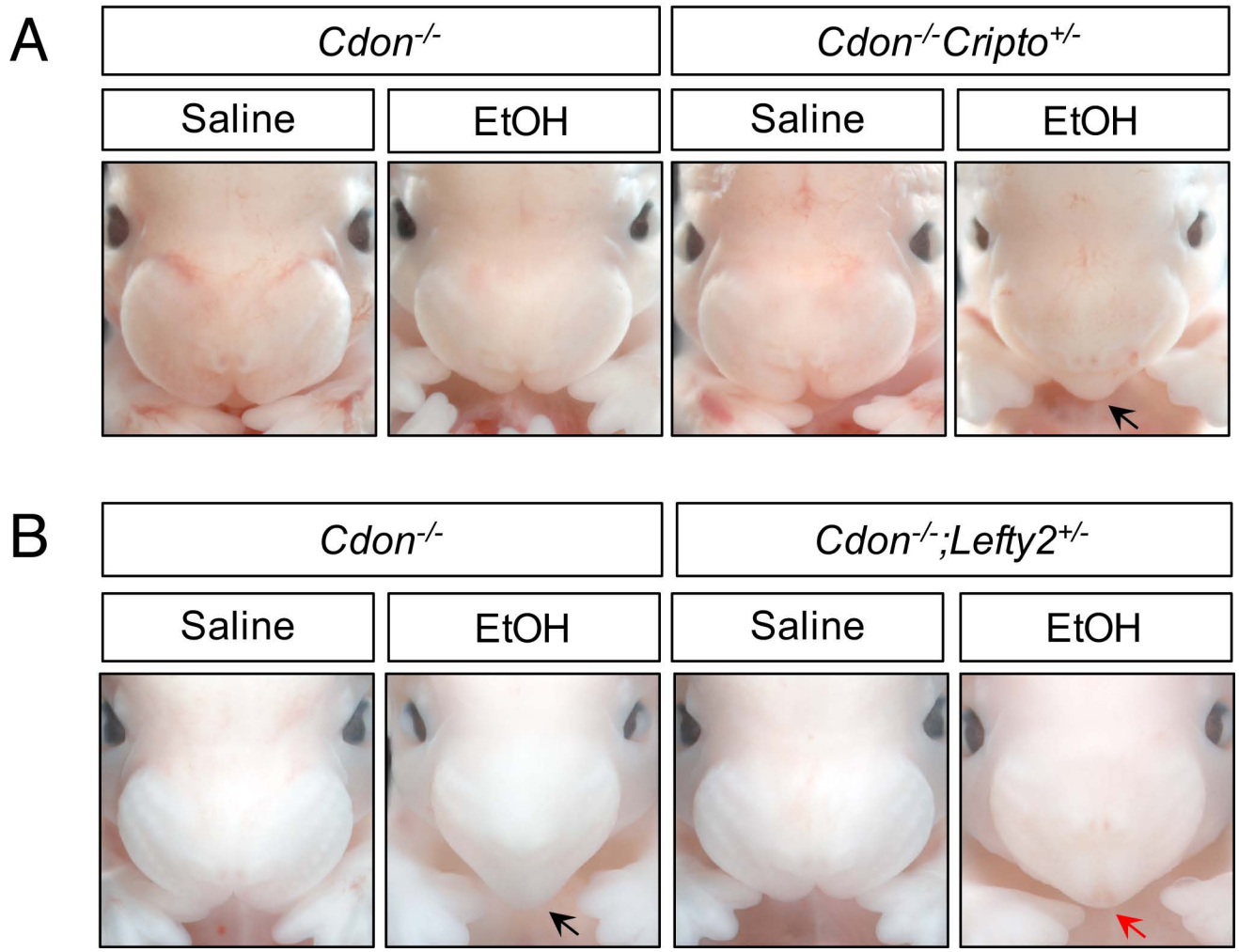

Figure S1. *Cripto* Heterozygosity Enhances, and *Lefty2* Heterozygosity Suppresses EtOH-Induced HPE in *Cdon*$^{-/-}$ Embryos

(A) Frontal views of E14.0 embryos. Removal of one copy of *Cripto* enhanced the response of *Cdon*$^{-/-}$ embryos to a dose of 2.9 g/kg EtOH (see Table 2 for quantification). The EtOH-treated *Cdon*$^{-/-}$*;Cripto*$^{+/-}$ embryo displays a fused upper lip (arrow). (B) Frontal views of E14.0 embryos. Removal of one copy of *Lefty2* suppressed formation of single nostril in *Cdon*$^{-/-}$ embryos the response to a dose of 3.48 g/kg EtOH (see Table 3 for quantification). The EtOH-treated *Cdon*$^{-/-}$ embryo displays a fused upper lip and single nostril (black arrow), whereas the EtOH-treated *Cdon*$^{-/-}$*;Lefty2*$^{+/-}$ embryo has a fused upper lip and two nostrils (red arrow).

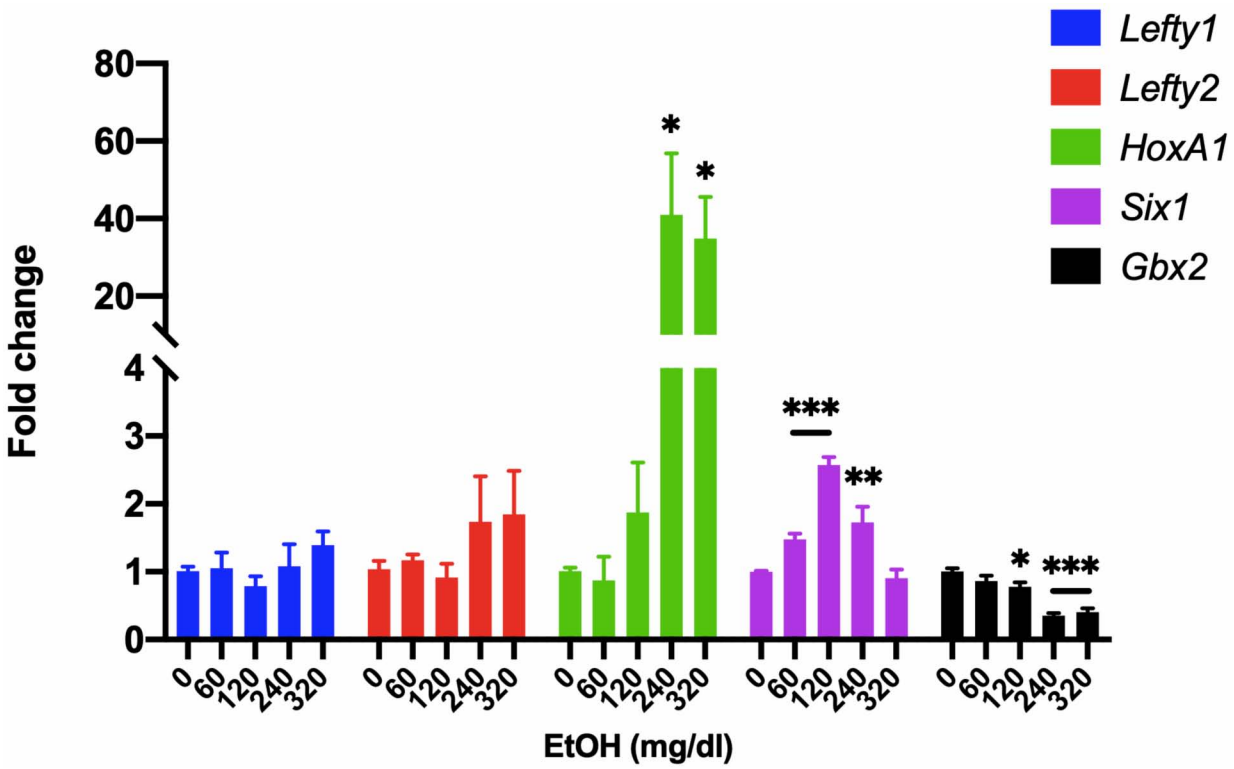

Figure S2. Analysis of gene expression in EtOH-treated mEpiSCs. qRT-PCR analysis of *Lefty1*, *Lefty2*, *HoxA1*, *Six1*, and *Gbx2* expression in mEpiSCs treated with the indicated doses of EtOH for 6 hours. Expression was normalized to *Gapdh* expression. N=3 experiments with two biological replicates in each experiment. Values for (B) and (C) are means ± SEM, *p<0.05, **p<0.01, ***p,0.001.

Table S1: PCR Primers

Primer	Sequence	Reference
Gapdh_F	AACGACCCCTTCATTGAC	(Dong et al., 2008)
Gapdh_R	TCCACGACATACTCAGCAC	(Dong et al., 2008)
Gbx2_F	GCAACTTCGACAAAGCCGAG	Harvard Primer Bank 133892275c2
Gbx2_R	CCTTGCCCTTCGGGTCATC	Harvard Primer Bank 133892275c2
HoxA1_F	CGCACAATGTTCTGATGTCC	(Matt et al., 2005)
HoxA1_R	TGCAAGCTTCATGACAGAGG	(Matt et al., 2005)
Lefty1_F	AACCGCACTGCCCTTAT	(Liu et al., 2018)
Lefty1_R	CGCGAAACGAACCAACTTGT	(Liu et al., 2018)
Lefty2_F	CAGCCAGAATTTTCGAGAGGT	(Liu et al., 2018)
Lefty2_R	CAGTGCGATTGGAGCCATC	(Liu et al., 2018)
Nanog_F	GGACTTTCTGCAGCCTTACG	(Chng et al., 2010)
Nanog_R	GCTTCCAAATTCACCTCCAA	(Chng et al., 2010)
Nodal_F	CCTGGAGCGCATTTGGATG	(Liu et al., 2018)
Nodal_R	ACTTTCTGCTCGACTGGACA	(Liu et al., 2018)
Oct4_F	AGTTGGCGTGGAGACTTTGC	(Liu et al., 2018)
Oct4_R	CAGGGCTTTCATGTCCTGG	(Liu et al., 2018)
SIX1_F	TTAAGAACCGGAGGCAAAGA	(Chng et al., 2010)
SIX1_R	GGGGGTGAGAACTCCTCTTC	(Chng et al., 2010)
Sox2_F	GCGGAGTGGAAACTTTTGTCC	(Liu et al., 2018)
Sox2_R	CGGGAAGCGTGTACTTATCCTT	(Liu et al., 2018)

Chng, Z., Teo, A., Pedersen, R.A., and Vallier, L. (2010). SIP1 Mediates Cell-Fate Decisions between Neuroectoderm and Mesendoderm in Human Pluripotent Stem Cells. Cell Stem Cell *6*, 59-70.

Dong, J., Sulik, K.K., and Chen, S.Y. (2008). Nrf2-Mediated Transcriptional Induction of Antioxidant Response in Mouse Embryos Exposed to Ethanol in vivo: Implications for the Prevention of Fetal Alcohol Spectrum Disorders. Antioxid Redox Signal *10*, 2023-2033.

Liu, C., Wang, R., He, Z., Osteil, P., Wilkie, E., Yang, X., Chen, J., Cui, G., Guo, W.e., Chen, Y.*, et al.* (2018). Suppressing Nodal Signaling Activity Predisposes Ectodermal Differentiation of Epiblast Stem Cells. Stem Cell Reports *11*, 43-57.

Matt, N., Schmidt, C.K., Dupé, V., Dennefeld, C., Nau, H., Chambon, P., Mark, M., and Ghyselinck, N.B. (2005). Contribution of cellular retinol-binding protein type 1 to retinol metabolism during mouse development. Dev Dyn *233*, 167-176.